Diplomarbeit

Determination of Power Curves of Wind Turbines using the Remote Sensing Technology LIDAR

ausgeführt zum Zwecke der Erlangung des akademischen Grades
eines Diplom-Ingenieurs unter der Leitung von

Univ.-Prof.i.R. Dipl.-Ing. Dr.techn. Erich Rummich
Institut für Energiesysteme und Elektrische Antriebe (E370)

eingereicht an der Technischen Universität Wien
Fakultät für Elektrotechnik und Informationstechnik

von

Christian Hofstetter, BSc.
Matrikelnummer 0525440
Ziegelhofstraße 36/5/23
1220 Wien

Wien, im März 2011

Acknowledgement

I would like to express my gratitude to all the employees of the VERBUND Renewable Power GmbH, who enabled me to gain practical experience in the field of renewables. Special thanks goes to Mr. Dipl.-Ing. Dr. Rudolf Zauner, who never hesitated to spend his time providing instructions and advice. Still he also allowed me to work self contained and freely.

I would like to thank my instructor from the Vienna University of Technology, Mr. Univ.-Prof.i.R. Dipl.-Ing. Dr. Erich Rummich. As the thesis deals with multi disciplinary contents the search of an instructor turned out to be far more difficult than expected. Fortunately, he is not only an expert in many technical disciplines but also a patient and warmhearted instructor. Therefore, he agreed to supervise this thesis.

I also acknowledge the support I have received due my social environment. Friends, offering understanding when time shortages led to reduced contact, sharing the pleasures of life and providing inspiring input whenever needed, contributed significantly to my personal growth.

Thanks to Robert, who not only offered grammatical corrections on my thesis, but also is a part of my family. This family was the basis allowing me my studies. My parents did every conceivable effort to support me on my way. Their passion cannot be honored accordingly. And also thanks to my dear sister, helping me everytime I ask her to.

Abstract

The scope of this master thesis is to determinate the power curves of wind turbines using the unconventional technology called light detection and ranging (LIDAR). LIDAR is a Remote Sensing Technology, which offers many advantages when measuring wind speed. Appliances can be easily installed in a given area, no building license is needed and the resolution of the measurement is higher than the one gained with conventional anemometer masts. Given these advantages the Austrian Electricity Company VERBUND conducted a project in which a LIDAR system was used for the determination of a power curve.

This thesis contains a basic description of wind utilization, a detailed physical description of LIDAR systems (theoretical principles chapter 3) and the documentation and evaluation of a series of measurements. Further aspects of volume measurements are considered allowing a comparison with conventional anemometer technology and providing a prospective outlook of LIDAR systems. Lastly, the crucial findings of the work are gathered in the conclusions of this thesis.

Formula Symbols

Symbol	Value	Unit	Description
A	–	m^2	area
A_{wdf}	–	1	parameter of a weibull probability density function
A_1	–	m^2	area in front of the converter
A_2	–	m^2	area behind the converter
a	–	m/s	offset in velocity azimuth display technique (VAD)
B	–	Vs/m^2	magnetic flux density
b	–	m/s	absolute value of the horizontal wind speed
c	$2.998 \cdot 10^8$	m/s	speed of light in vacuum
c_p	–	1	power coefficient
D	–	As/m^2	electric flux density
E	–	V	electric field strength
E_{kin}	–	J	kinetic energy
E_{nrg}	–	J	energy of a photon
E_{pot}	–	J	potential energy
E_0	–	V	electric field strength in air
e	$1.602176487 \cdot 10^{-19}$	As	elementary charge
F	–	N	force
F_c	–	N	coulomb force
F_{cf}	–	N	centrifugal force
f	–	s^-1	frequency
G	–	$1/m^2$	geometry factor

H_0	–	A/m	magnetic field strength
h	$6.62606896 \cdot 10^{-34}$	Js	planck constant
I	–	A	electric current
I_c	–	W/m^2	intensity of the collected signal
I_s	–	W/m^2	intensity of the scattered signal
I_0	–	W/m^2	emitted intensity
J	–	A/m^2	electric current density
K	–	Wm^3	system factor
k	–	rad/m	wave number
k_{wdf}	–	1	parameter of a weibull probability density function
l	–	m	length
M	–	A/m	magnetization
m	–	kg	mass
m_e	$9.10938215 \cdot 10^{-31}$	kg	rest mass of an electron
N	–	1/m^3	number concentration
n	–	1/m^3	density of free electrons
n_i	–	1/m^3	particle density for intrinsic conduction
n_n	–	1	main quantum number
O	–	1	overlap function
P	–	W	power
P_z	–	As/m^2	electric polarization
p	–	1/m^3	density of electron holes
p_r	–	N/m^2	air pressure
p_x	–	kgm/s	mechanical momentum
R_m	287.058	J/(kgK)	specific gas constant for air
R	–	m	distance
r	–	m	radius
S	–	W/m^2	electric energy flux density
s	–	1	slip of asynchronous machines
s_1	–	1	signal 1
s_2	–	1	signal 2
T	–	K	absolute Temperature

T_t	$-$	1	transmission coefficient
t	$-$	s	time
V	$-$	m^3	volume
v_{norm}	$-$	m/s	normalized wind speed
v_1	$-$	m/s	undelayed free stream velocity
v_2	$-$	m/s	velocity behind the converter
v'	$-$	m/s	flow velocity through the converter
wdf	$-$	1	probability density function
x	$-$	m	length in x-axis direction (cartesian coordinates)
y	$-$	m	length in y-axis direction (cartesian coordinates)
Z_{w0}	376.730313461	V/A	characteristic wave impedance
z	$-$	m	length in z-axis direction (cartesian coordinates)
α	$-$	1/m	extinction coefficient
β	$-$	1/(m sr)	backscattering coefficient
δ	$-$	1	dirac impulse
$\hbar$	$1.054571628 \cdot 10^{-34}$	Js	planck constant divided by 2π
η_{system}	$-$	1	degree of efficiency of a wind power plant
ε	$-$	As/Vm	permittivity
ε_0	$8.8541878176 \cdot 10^{-12}$	As/Vm	dielectric field constant
ε_r	$-$	1	relative permittivity
λ	$-$	m	wavelength
λ_v	$-$	1	tip speed ratio
μ	$-$	Vs/Am	permeability
μ_0	$4\pi \cdot 10^{-7}$	Vs/Am	magnetic field constant
μ_r	$-$	1	relative permeability
$\vec{\nabla}$	$-$	-	vectorial differential operator
ψ	$-$	1	wave function
ρ	$-$	kg/m^3	density
ρ_0	1.225	kg/m^3	standardized air density
ρ_h	$-$	kg/m^3	measured density

σ	–	m^2/sr	scattering cross section
θ	–	rad	azimuthal angle
τ	–	s	pulse time
Φ	–	rad/s	control variable
ϕ	–	rad	polar angle
ω	–	s^{-1}	angular frequency

Contents

Chapter 1

Introduction

Wind is an essential part of the earth´s ecosystem earth. With the ability to move large amounts of air it influences life in many ways. Be it the carnivore considering wind direction and speed to reduce the risk of being detected due to smell, plants growing seeds designed for wind dispersion or the influence of wind on climate and weather conditions. Human interest in wind therefore always existed. The first technical utilizations included sailing ships and wind mills. Times have changed, but wind utilization remains a current topic. Nowadays wind turbines are used to convert kinetic wind energy into electric energy. Knowledge of the wind speed is crucial for wind farm design as well as power curve assessment.

Wind speeds are conventionally measured by anemometers. Within the last decade new technology has appeared: light detection and ranging (LIDAR). The scope of this master thesis is to determinate the power curves of wind turbines using LIDAR. LIDAR is a remote sensing technology which offers many advantages concerning wind speed measurements: appliances can be easily installed in a given area, no building permission is needed and the resolution of the measurement is higher than the one gained with conventional anemometer masts. Given these advantages the Austrian Electricity Company Verbund conducted a project in which a LIDAR system was used for the determination of power curves.

This thesis contains a brief description of the topic of wind utilization. Herein the topic of wind energy as well as the principle of energy conversion based upon wind turbines is explained. A detailed physical description of LIDAR systems (theoretical principles section 3) allows a deeper understanding of its principles. The opportunities and limits of LIDAR technology are discussed. A comparison with the competing technology, sonic detection and ranging (SODAR), is also done.

Based upon fundamental physical description of wind utilization and LIDAR systems the measurement campaign is described. Formal and technical requirements contained in this thesis were either obtained from IEC 61400-12 or derived within this project. The measurement campaign lasted for a total of 2 months and provided sufficing data for crucial insights. The questions to be answered included:

- Does LIDAR technology meet the requirements for site assessment and power curve determination?
- If so, how shall power curve determination be done?
- What influence do variations of the power curve have on the energy yield under certain wind conditions?

Consideration of future developments leads to an outlook and a final discussion indicating a scenario of prospective LIDAR systems. Lastly, the crucial findings of the campaign are gathered in a short summary leading to the conclusions of this thesis.

Chapter 2

Wind Utilization

Wind energy in general represents kinetic energy stored in the movement of air mass. This mass flow is caused due to global differences in temperature and pressure as a consequence of solar irradiation as well as heat radiation dissipated from the earth back into the atmosphere. Wind turbine generators convert a part of this wind energy into electrical energy. There are many different applied generator concepts - the most important of which are briefly explained in section 2.3.

2.1 Wind Power

The kinetic energy, E_{kin} $[J]$, of mass, m $[kg]$, is defined as:

$$E_{kin} = \frac{mv^2}{2} \tag{2.1.1}$$

Assuming a certain cross-sectional area, A $[m^2]$, through which air mass flows with a certain velocity, v $[m/s]$, the volume, V $[m^3]$, passing the area within a unit of time is called volume flow $\dot{V}$:

$$\dot{V} = vA \tag{2.1.2}$$

As the volume is filled with matter, a mass flow can be defined using the air density ρ $[kg/m^3]$:

$$\dot{m} = \rho v A \tag{2.1.3}$$

The mass passing the area A within a certain time contains kinetic energy. The physical power is determined by the mass flow of matter $\dot{m}$ passing through the area:

$$P = \frac{\dot{m}v^2}{2} = \frac{\rho A v^3}{2} \tag{2.1.4}$$

It is essential to recognize the relation of the physical power and the velocity: The physical power increases with the velocity to the power of three. Knowledge concerning the wind velocity and its distribution in a given area is therefore of great value and serves as the basic principle to assess specific sites for wind turbine generator placement. Errors and inaccuracies can be of great influence because the velocity measurement is increased by a power of three.

2.2 Power Coefficient

Wind turbine generators convert kinetic energy into electric energy due the slowdown of the air mass. No slowdown of the velocity would mean no wind resistance of the turbine and therefore no energy conversion. If the velocity on the backside would be zero, no mass would flow through the converter leading to the same result. The Power Coefficient c_p [1] is an indicator for the ratio of converted power to kinetic energy flow.

As air is a continuum, the velocity of the wind changes continuously. Figure 2.2.1 shows the flow conditions due to the extraction of kinetic energy from a free-stream air flow. v_1 is the undelayed free-stream velocity, v_2 is the flow velocity far behind the converter and v' is the flow velocity through the converter.

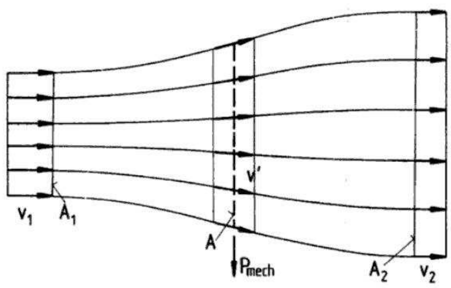

Figure 2.2.1: Flow conditions due to the extraction of mechanical energy from a free-stream air flow, according to the elementary momentum theory, [1]

The power converted by the turbine corresponds to the power difference before and after the converter:

$$P = \frac{\rho A_1 v_1^3}{2} - \frac{\rho A_2 v_2^3}{2} = \frac{\rho}{2}\left(A_1 v_1^3 - A_2 v_2^3\right) \tag{2.2.1}$$

Maintaining the mass flow requires that:

$$\rho v_1 A_1 = \rho v_2 A_2 \tag{2.2.2}$$

leading to:

$$P = \frac{\dot{m}\left(v_1^2 - v_2^2\right)}{2} \tag{2.2.3}$$

The conservation of momentum requires a thrust force:

$$F = \dot{m}\left(v_1 - v_2\right) \tag{2.2.4}$$

Resulting in a power:

$$P = Fv' = \dot{m}\left(v_1 - v_2\right)v' \tag{2.2.5}$$

Equating 2.2.3 and 2.2.5 leads to:

$$v' = \frac{v_1 + v_2}{2} \tag{2.2.6}$$

And therefore the flow velocity through the converter equals the arithmetic mean.

The mass flow trough the converter can now be defined as:

$$\dot{m} = \rho A v' = \rho A \frac{v_1 + v_2}{2} \tag{2.2.7}$$

Inserting this mass flow into equation 2.2.3 results in:

$$P = \frac{1}{4}\rho A\left(v_1^2 - v_2^2\right)\left(v_1 + v_2\right) \tag{2.2.8}$$

If the power within the mass flow in the Area A distant from the converter equals $P_o = \rho v_1^3 A/2$ $[J/s]$, then the power coefficient can be calculated as:

$$c_p = \frac{P}{P_0} = \frac{\rho A\left(v_1^2 - v_2^2\right)\left(v_1 + v_2\right)}{2\rho A v_1^3} \tag{2.2.9}$$

and reaches a maximum of $c_{p,betz} = 16/27$ for $v' = 2/3v_1$ and $v_2 = 1/3v_1$.

2.3 Wind Turbines

The direct human use of wind power can be traced back thousands of years, for instance the use of ships equipped with sails. The first historical proven wind mill dates from the year 644 AD and its purpose was to mill grain. Electricity became commercially available with the construction of power plants (the very first one was built in the year 1882 AD in New York). The first wind energy turbine generator producing electricity was founded in the year 1891 AD (Denmark). A long lasting stage of development followed in the next decades. The design concepts had been many and diverse. Some wind turbines had two blades, some rotated horizontal, some converted the energy due to drag forces, others due to lift. The electrical concepts had also been various. DC machines, synchronous machines and asynchronous machines had been tested. Nowadays, just a few different concepts have proven competitive- the most important ones are briefly explained in chapter 2.3.3. The basic components of wind turbines generators are as follows:

2.3.1 Components

Foundation

The foundation provides mechanical support for the tower and wind turbine and must be designed to withstand potentially very strong wind forces. The design and costs for the foundation depends on the ground conditions.

Transformer

Most wind turbine generators are feeding the electricity into a medium-voltage power grid. As the systems run at lower voltage levels a transformer provides the proper output voltage.

Tower

Towers for large wind turbines may be either tubular steel towers, lattice towers, or concrete towers.

Nacelle

The nacelle contains the most sensitive parts of a wind energy systems. It comprises the generator (depending on the system this may also include a gearbox), yaw motors, the adapter to fix the blades and the spinner, blade pitch motors, normally a load winch and a cooling fan. Figure 2.3.1 shows an example of a wind turbine by Enercon.

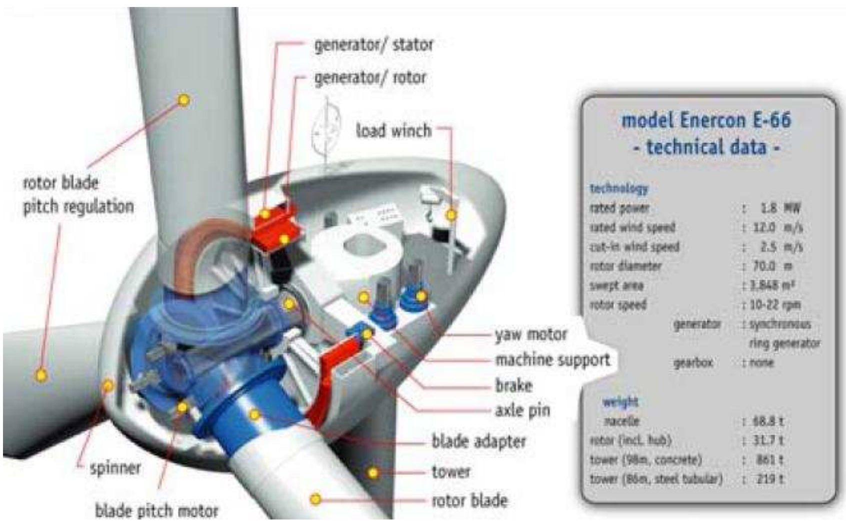

Figure 2.3.1: Nacelle of the wind turbine by Enercon (E66, 2006), [2]

Blades

Due to the high tip speeds blades are made of glass-fibre-reinforced polyester (GFRP) or carbon-fibre-reinforced plastics (CFRP). CFRP is more expensive but its fatigue strength is three times higher than GFRP. Nowadays, the rotor consists of three blades using lift forces and no drag (the maximum power coefficient of a pure drag type rotor becomes $c_{max} \approx 0.2$). Figure 2.3.2 and 2.3.3 show a principal schematic of the lift forces and its origin. The power coefficient depends on the wind speed and the shape of the blade and is limited in the best case to $c_{p,betz}$. Due to the rotational wake of the passing air, a part of the kinetic energy cannot be converted (see figure 2.3.4). Figure 2.3.5 shows the results of the calculation done by Schmitz.

λ_v represents the tip speed ratio and is defined by:

$$\lambda_v = \frac{v_{blade,tip}}{v_{wind}} \tag{2.3.1}$$

Depending on the tip speed ratio, each rotor reaches its maximum power coefficient in one specific working point. Figure 2.3.6 gives an overview of c_p- curves for different numbers of rotor blades.

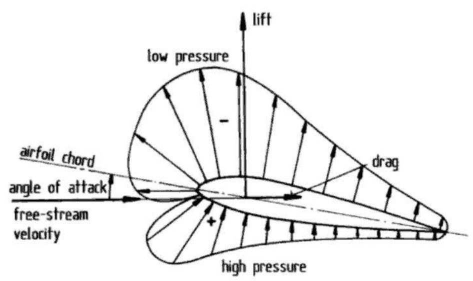

Figure 2.3.2: Aerodynamic forces acting on an airfoil exposed to an air stream, [1]

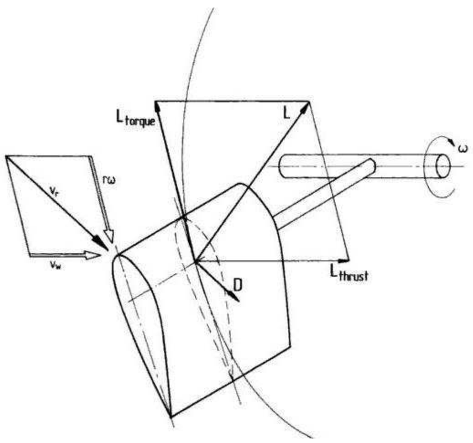

Figure 2.3.3: Flow velocities and aerodynamic forces acting on a propeller-like rotor, [1]

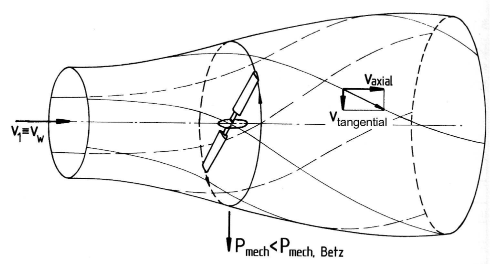

Figure 2.3.4: Extended momentum theory, taking into consideration the rotating rotor wake, [4]

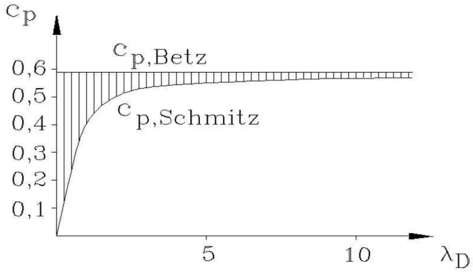

Figure 2.3.5: Power coefficient calculated by Schmitz, [2]

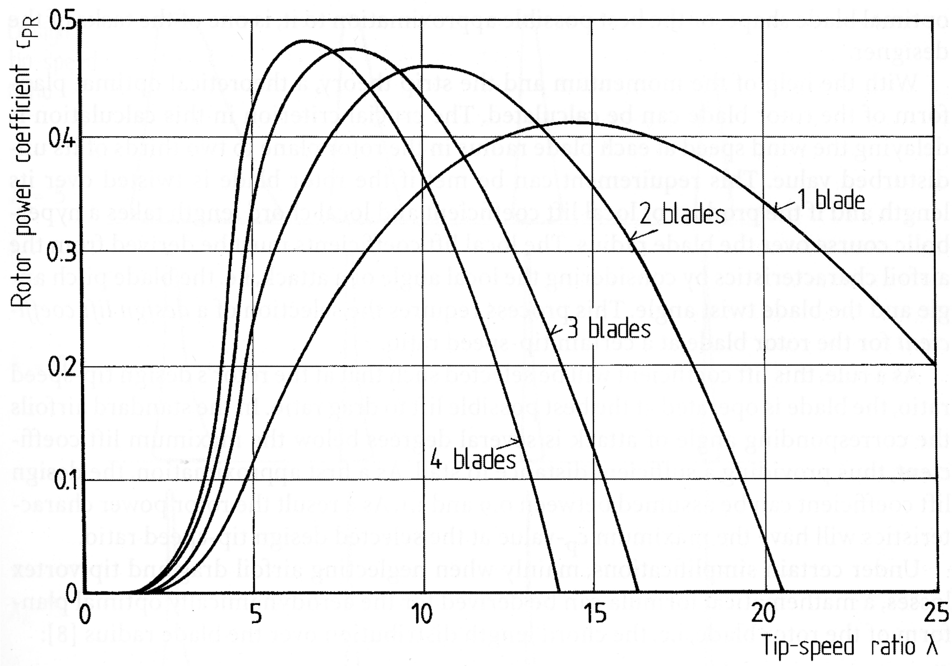

Figure 2.3.6: Influence of the number of blades on the rotor power coefficient and the optimal tip speed ratio, [3]

2.3.2 Power Control

At high wind speeds the mechanical power of the rotor would exceed the limits demanded by the mechanical and electrical wind power system. Therefore, the mechanical power of the rotor needs to be limited. All modern rotor blades use lift forces and the derived blade profile shape is like the one in figure 2.3.2. Keeping in mind the vectors of the flow velocities, aerodynamic forces (see figure 2.3.3 and the calculations done in section 2.1 four options for aerodynamic power regulation are possible:

- change of the projected swept area of the rotor due to yawing
- change of the rotor speed leading to a different relative flow velocity v_r
- change of the attack angle (pitch)
- blade profiles reducing the power coefficient with increasing wind speeds (stall)

In case of storms, modern turbines turn out of the wind direction and in this way reduce the projected swept area of the rotor to almost zero (the process of yawing, the cutoff wind speed determines wether the turbine needs to be shut down or not). If the wind speeds are higher than necessary for full load operation but not high enough to initiate cutoff, the mechanical power still needs to be limited to full load. The power range which can be controlled by changing rotor speed is very limited. Therefore, wind turbines typically use the concept of stall or pitch regulation whereas pitch regulation has been found superior in modern concepts. Figure 2.3.7 shows a comparison of the power curve (a detailed description of power curves follows in chapter 2.3.4) of both concepts.

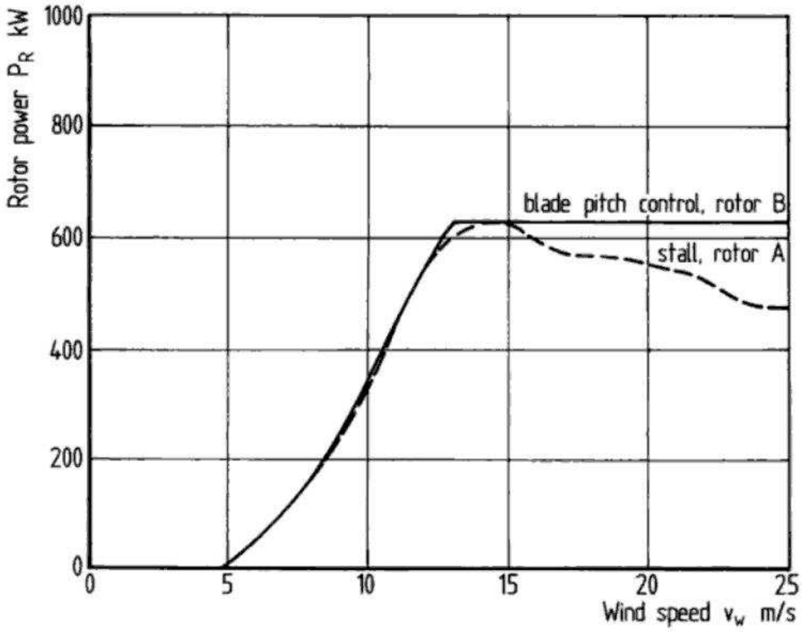

Figure 2.3.7: Power output versus wind speed (power curve) of a stall-limited rotor (A) and a rotor with continuous blade pitch control (B), [2]

As already mentioned the mechanical momentum obtained by a rotor can also be varied by the change of the attack angle. The dynamic change of the attack angle of the rotor blades is commonly known as pitching. Most of the modern wind turbines are using this technology. The constant power output of pitching systems justifies the additional technological efforts demanding pitch motors and an automated regulation system.

In contrast stall regulated WTG's don't show a constant power curve. Still the concept of stall is a cheap and effective power regulation method. It allowed the first economical reasonable wind power projects and therefore contributed strongly to the success of WTG's in past.

2.3.3 Electrical Systems

The electrical system of a wind turbine generator must contain at least an electrical generator. The generator converts mechanical power into electrical power. All common generators are generating its mechanical forces by the use of the Lorentz force F $[N]$, which claims:

$$\vec{F} = Il\vec{e}_l \times \vec{B} \tag{2.3.2}$$

The mechanical forces are therefore proportional to the magnetic flux density B $[Vs/m^2]$ as well as the electric current I $[A]$ and the length l $[m]$ of the conductor. The outer product shows also a dependence of the angle between the vectors $\vec{e_l}$ and $\vec{B}$. Static magnetic fields are containing the energy density:

$$E_m = \frac{BH}{2} \tag{2.3.3}$$

The concept of entropy postulates the rise of the entropy in each process within closed systems and continuing time. Therefore the Lorentz force can be seen as a magnetic force obtaining energy minimums within magnetic fields.

Most concepts of electrical motors and generators can be distinguished by the way they generate magnetic and electrical fields as well as currents leading finally to the Lorentz force. Three different motor and generator concepts are nowadays common if the mechanical power exceeds several kilowatts.

Direct Current Machines

Direct Current Machines (DC Machines) are feed by direct current. The magnetic field within the machine stays more or less constant in space and time. Brushes and commutators are connecting the armature winding with the electrical source. Electrical power grids are usually run by alternating current. Therefore the use of DC Machines in WTG's was not common. Nowadays electronic devices allow the conversion of direct current into alternating current. Still the average degree of efficiency and the operating characteristics disqualify the DC Machine for wind power application if it is compared with the following machines.

Asynchronous Machines

The first competitive wind turbine generator concept based on asynchronous machines and stall regulation. It spread widely known as the "Danish concept" and started a successful market penetration. The asynchronous machine had been in favor for its specific way of operation. It complemented the technological possibilities given in the beginning of WTG's best. In contrast to the Direct Current Machine the Asynchronous Machine runs by alternating current, generating a rotating magnetic field within the stator. If the rotor spins synchronously with this field, the magnetic state of the rotor stays constant in time. If the number of revolutions per minute is different (asynchronous), the magnetic field within the rotor is changing. Equation 3.1.4 claims electric fields as a result of changing magnetic fields. This is also true for magnetic fields within machines, leading to electric fields causing electric currents in the rotor. Depending on the phase shift of the current a mechanical momentum appears. For the use in WTG's, two special attributes of the Asynchronous Machine can be pointed out:

First, the machine does not need to rotate synchronous with the feeding field, moreover, it demands a relative motion in order to create a momentum. The relative motion is described by the slip (equation 2.3.4).

Second, the Asynchronous Machine does not need brushes connecting the electric source with the rotor (cage rotor asynchronous machines). Still many modern systems are using brushes in order to influence the electric state of the rotor as well as its electric resistance (slip ring asynchronous machines). The manipulation of the electric field within the rotor allows to influence the torque as well as the reactive power of the generator. The number of pole pairs in connection with the frequency of the feeding electrical source defines the synchronous number of revolutions. As asynchronous machines are based upon electromagnetic induction sufficing changes of the magnetic flux density is necessary. This limits the realized synchronous number of revolutions to values still demanding a gear box in order to connect with the comparably slow circling rotor. Many modern WTG's are equipped with so called "Double-Fed Induction Generators" (see figure 2.3.8). These are slip ring asynchronous machines as already described before. The rotor is connected to an inverter allowing the systematic manipulation of the rotor field.

The advantages of these systems are:

- the operational slip of the generator can be varied by approximately ±30% [1] allowing a speed variation of the rotor
- the mechanical momentum of the generator can be varied by a field oriented control
- the reactive power of the asynchronous machine can be varied by a field oriented control
- electrical power generated in the rotor can be fed back into the grid increasing the overall efficiency

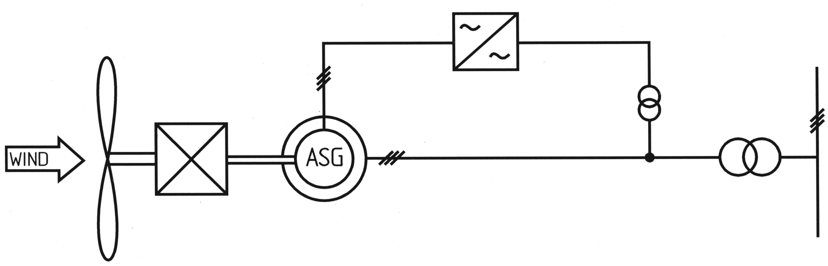

Figure 2.3.8: Double-fed induction generator, [4]

$$s = \frac{n_{syn} - n_{mech}}{n_{syn}} \tag{2.3.4}$$

[1]the operational slip of conventional asynchronous machines limited to a maximum of 5% in order to keep a high degree of efficiency

Synchronous Machines

The synchronous machine is the most common generator in power plants. Hydro power plants, nuclear power plants as well as thermal power plants are normally equipped with synchronous machines offering a wide range of power output (from several kW up to several 100 MW). The benefits of the synchronous machines are a high degree of efficiency and a simple controllability of the mechanical and the reactive power. In case of WTG's the characteristics of synchronous machines had been improper in past. Since the advance of electronic converters concepts based upon synchronous machines are gaining importance.

The principal of the stator of the synchronous machine is similar to the asynchronous machine. Alternating currents in the electric coils are generating a rotating magnetic field within the stator. In contrast to the asynchronous machine the rotor is fed with direct currents, generating a constant field within the rotor coordinate system. The rotor acts as a magnet which follows the synchronous field created by the stator. The angle between the stator current and the resulting field is responsible for the mechanical momentum generated by the system. Synchronous machines are supposed for operating polar wheel angles far below 90°. Otherwise the machine might exceed its maximum mechanical moment leading to forbidden operating state.

The strict connection of the frequency of the feeding grid and the rotation speed of the synchronous machine delayed a successful use in WTG's. Nowadays electronic converter allow the variation of the feeding frequency. This allows various speed operation of the synchronous machine leading to proper operating characteristics. Older converters demanded considerable reactive power and had a significant influence on the overall degree of efficiency. As the properties of modern converters are improving constantly WTG's based upon synchronous machines are now competing with WTG's based upon double-fed induction generators. The german company Enercon has developed synchronous machines with unconventional high numbers of pole pairs (72 in case of the model E66 from the year 2005). This allows the abandonment of a gear box (a schematic of the electrical system can be seen in figure 2.3.9). On the other hand the generator is voluminous, heavy and partly integrated into the spinner. Therefore the whole design of the nacelle and the spinner is adapted to the dimensions of the generator. Each generator showing different dimensions therefore requires a specific spinner and nacelle design. As the weight of the nacelle increases the tower of the WTG needs to suffice higher mechanical loads.

The advantages of the system are:

- variable speed operation is possible
- the mechanical momentum of the generator can be varied by a field oriented control
- the reactive power of the synchronous machine can be varied by a field oriented control (due the stator) or the manipulation of the rotor current

- a gearbox is not necessary if the synchronous machine has accordant number of pole pairs

The disadvantages of the system are:

- the raise of weight requires an extensive construction of the basement and the tower
- the nacelle and the spinner needs to be adapted to the dimensions of the generator
- the electronic converter converts the whole power fed into the grid
- the price increase due higher requirements concerning the mechanical load and the converter and costs for the individual spinner and nacelle design

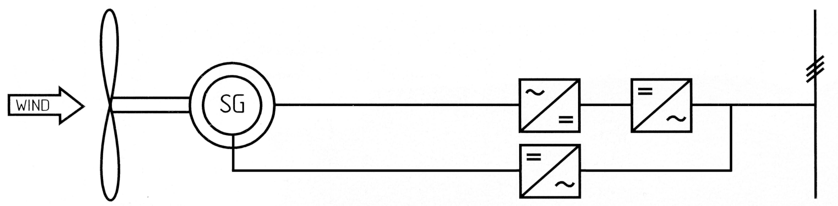

Figure 2.3.9: Directly rotor-driven variable-speed synchronous generator with frequency inverter, [4]

Finally synchronous machines with permanent magnets need to be mentioned. In this case the stator stays the same as described before but the rotor carries permanent magnets instead of electric coils. This allows the abandonment of the slip ring and the rotor current. As a consequence degree of efficiency increases slightly. On the other hand the level of the magnetic field generated by the rotor cannot be manipulated. Still field oriented control allows sufficient controllability. The use of permanent magnets allows very high energy densities within the machine which leads to very compact machines, which is another advantage of the permanent magnet synchronous machine. Up to now the manufacturing of highly magnetized permanent magnets is very expensive. Progresses in material sciences may boost the permanent magnetic synchronous machine to a dominant market position in future.

2.3.4 Power Curves

The electrical power output versus the wind speed is referred to as the power curve of a WTG. One example of power curve has already been shown in chapter 2.3.2 (figure 2.3.7). It is the essential characteristic of each WTG and allows to make predictions concerning the energy yields if site assessment needs to be done. Therefore it is of great importance for choice of the fitting on a given wind site. These power curves are normally guaranteed by the manufacturer, leading to reduced investment risks, lower risk add-ons and a higher bank ability. From a technical point of view modern wind farm planning affords detailed information about the power curve of WTGs, standardized measuring methods of the wind speeds on the specific site as well as the proper arrangement of the WTGs minimizing losses due wind shadows.

If the power coefficient versus the wind speed of a WTG is known, the power output can be calculated mathematically by:

$$P(v) = c_P(v)\eta_{system}\frac{\rho A v^3}{2} \tag{2.3.5}$$

The atmospheric conditions are defined by DIN 5450 (air density $\rho_0 = 1,225 kg/m^3$). The degree of efficiency (η_{system}) includes all losses starting with the mechanical momentum on the rotor down to the energy conversion in the electronic inverter. The efficiency of the transformer is normally excluded.

Nowadays power curves are not just calculated mathematically but also measured physically. The directive IEC 61400-12 gives an authoritative instruction for the measurement of power curves. The cut in speed, rated operating speed and the cut off speed determines the speed range of the measurement. The geometrical shape of a power curve of a WTG can vary due rotor losses and differences in the power control setup. Therefore the guarantee of the power curve does not concern the exact shape of the curve but guarantees a mathematical calculated energy yield within a given wind field.

Under real conditions the shape of the ground surface, shadowing effects due other WTGs and different air density due humidity, temperature and height have influence on the measured power curve and need to be considered.

If air is considered as an ideal gas the density is defined due:

$$\rho = \frac{p_r}{R_m T} \tag{2.3.6}$$

The variable p_r $[N/m^2]$ represents the pressure, R $[J/kgK]$ represents the gas constant and T $[K]$ stands for the absolute temperature. As the gas constant of water vapor is higher than the gas constant of dry air, the humidity also has influence on the air density. Still the humidity has not to be determined during a measurement campaign.

2.4 Wind Speed Measurement

The reliable measurement of wind speeds was up to know done by the use of cup anemometers. A class 1 anemometer shall not deviate more than 1% in wind speed from an 'ideal anemometer' response measuring the horizontal component of the wind speed. Still different design concepts led to differences up to 4% in wind speed on free field leading to differences in wind power up to 12,5% which was insufficient for the purpose of site assessment and the determination of power curves. Nowadays the directive IEC61400-12-1 sets the classification standards for cup anemometers.

Anemometers are capable to measure the wind speed in a certain spot within space. LIDAR's in contrast are capable to measure several velocities within a volume. Therefore the requirements LIDAR's need to fulfill cannot be the same. The use of LIDAR technology for the purpose of wind speed measurement claims a homogenous air stream within the illuminated volume. Turbulence within the volume decreases the accuracy significantly leading to limited eligibility in uneven terrain. Still further developments like the change of the scanning cone angle allows to reduce the inaccuracies claiming a bright future of wind LIDAR's.

Chapter 3

Physical Fundamentals of LIDAR Systems

Light Detection and Ranging (LIDAR) systems obtain information about the atmospheres by emitting and detecting electromagnetic waves. A physical description of electromagnetic waves will first be described (section 3.1) providing a common foundation for further understanding.

In the case of LIDAR systems semiconductors are used to convert electromagnetic waves into directly measurable electrical signals. The interaction of light and matter will be described within the chapter Semiconductor Physics (section 3.2). A short description of the concept of Quantum Mechanics is used to explain partly Bohr‘s Atomic Model leading to the energy model of semiconductors. Finally, a brief description of direct and indirect semiconductors shall allow the understanding of the conversion of electromagnetic waves into potential energy and *vice versa* within semiconductors which is a global affair if we think about light emitting diodes and photovoltaic cells.

The chapter Semiconductor Physics (section 3.2) describes the interaction of electromagnetic waves with contents of the atmosphere. This leads to a basic understanding how information can be obtained using LIDAR systems.

3.1 Electromagnetic Waves

Electromagnetic waves interact with their environment. The theory of electrodynamics gives a complete physical description of electromagnetic waves (more see section 3.1.1 and 3.1.2). Whereas continuous energy density spectrums are dominant on the macroscopic scale, the energy E_{nrg} can be quantified on the microscopic scale as a sum of single photons containing the energy:

$$E_{nrg} = \hbar\omega \tag{3.1.1}$$

ω $[1/s]$ represents the angular velocity. The emission and detection of photons is done by the change of discrete energy levels within atoms. A short description of these mechanisms can be found in section 3.2.

3.1.1 Maxwell Equations

The constitutive relations between the fields $\vec{E}$ $[V/m]$ (electric field strength) and $\vec{D}$ (electric flux density) as well as $\vec{H}$ $[A/m]$ (magnetic field strength) and $\vec{B}$ (magnetic flux density) allows under certain circumstances the simplification of the Maxwell Equations leading to a specific wave equation. The electric properties of materials are represented by their relative permittivity ε_r [1] and their relative permeability μ_r [1] which allow the definition of an electric and a magnetic polarization ($\vec{P}_z$ $[As/m^2]$ and $\vec{M}$ $[A/m]$). The magnetic constant μ_0 is determined by the definition of the Ampere, the unit of the electric current. It is defined as $\mu_0 := 4\pi \cdot 10^{-7} Vs/Am$. The electric constant is determined by the maxwell relation: $\varepsilon_0 = \frac{1}{\mu_0 c_0^2} \approx 8.854 \cdot 10^{-12} As/Vm$. $\vec{J}$ $[A/m^2]$ and $\vec{D}$ $[As/m^2]$ represent the electric current density and the electric flux density.

The constitutive relations are first described and afterwards integrated into the Maxwell Equations.

Constitutive relations:

$$\vec{D} = \varepsilon \vec{E} = \varepsilon_0 \vec{E} + \vec{P}_z \qquad \varepsilon = \varepsilon_0 \varepsilon_r \tag{3.1.2}$$

$$\vec{B} = \mu \vec{H} = \mu_0 \left[\vec{H} + \vec{M} \right] \qquad \mu = \mu_0 \mu_r \tag{3.1.3}$$

Maxwell Equations in matter:

$$\vec{\nabla} \times \vec{E} = -\mu_0 \left[\frac{\partial \vec{H}}{\partial t} + \frac{\partial \vec{M}}{\partial t} \right] \tag{3.1.4}$$

$$\vec{\nabla} \times \vec{H} = \varepsilon_0 \frac{\partial \vec{E}}{\partial t} + \frac{\partial \vec{P}_z}{\partial t} + \vec{J} \tag{3.1.5}$$

$$\vec{\nabla} \cdot \left[\varepsilon_0 \vec{E} + \vec{P}_z \right] = \rho_c \tag{3.1.6}$$

$$\vec{\nabla} \cdot \mu_0 \left[\vec{H} + \vec{M} \right] = 0 \tag{3.1.7}$$

with the vectorial differential operator in cartesian coordinates:

$$\vec{\nabla} = \vec{e}_x \frac{\partial}{\partial x} + \vec{e}_y \frac{\partial}{\partial y} + \vec{e}_z \frac{\partial}{\partial z} \tag{3.1.8}$$

In the case of LIDAR systems operating in the medium air several simplifications of the Maxwell Equations are feasible:

- the magnetic polarization is insignificantly low ($\vec{M} = 0$)
- the current density is insignificantly low ($\vec{J} = 0$)
- the charge density is insignificantly low ($\rho_c = 0$)

Therefore the rotation of the electric and magnetic field simplifies to:

$$\vec{\nabla} \times \vec{E} = -\mu_0 \frac{\partial \vec{H}}{\partial t} \tag{3.1.9}$$

$$\vec{\nabla} \times \vec{H} = \frac{\partial \vec{D}}{\partial t} \tag{3.1.10}$$

3.1.2 Propagation of Electromagnetic Waves

Based on descriptions within chapter 3.1.1 predictions concerning the propagation of electromagnetic waves are possible. Combining equations 3.1.9 and 3.1.10 gives the following wave equation:

$$\vec{\nabla} \times \left(\vec{\nabla} \times \vec{E}\right) = -\vec{\nabla} \times \mu_0 \frac{\partial \vec{H}}{\partial t} = -\mu_0 \frac{\partial^2 \vec{D}}{\partial t^2} \tag{3.1.11}$$

Using the identity:

$$\vec{\nabla} \times (\vec{\nabla} \times \vec{a}) = \vec{\nabla}(\vec{\nabla} \cdot \vec{a}) - \nabla^2 \vec{a} \tag{3.1.12}$$

and because $\vec{\nabla} \cdot \vec{E} = 0$ since $\rho = 0$ follows

$$-\nabla^2 \vec{E} + \mu_0 \frac{\partial^2 \vec{D}}{\partial t^2} = 0 \tag{3.1.13}$$

Inserting the Maxwell Relation $c_o := \frac{1}{\sqrt{\varepsilon_0 \mu_0}}$ finally leads to the wave equation where $c_o = 2.998 \cdot 10^8 m/s$ is the velocity of light in vacuum.

$$\nabla^2 \vec{E} - \frac{\varepsilon}{c_0^2} \frac{\partial^2 \vec{E}}{\partial t^2} = 0 \tag{3.1.14}$$

The wave equation connects the behavior of electromagnetical waves in space and time. A possible wave function that solves equation 3.1.14 in a single dimension is:

$$E(x,t) = Re\left[E_0 \cdot e^{j(kx - \omega t)}\right] \tag{3.1.15}$$

The parameter k $[rad/m]$ represents the wave number, the parameter ω $[rad/s]$ is called angular frequency.

The spread of an electromagnetic wave can now be described by the following parameters:

- the velocity c is defined by the Maxwell Relation
- the frequency $f = \frac{\omega}{2\pi}$depends on the energy of the emitted photons (further details see chapter 3.2.1)
- and the amplitude of the electric and the magnetic field is given through the characteristic wave impedance of the medium and the transmission power of the wave.

The characteristic wave impedance in the medium air is approximately equal to that in vacuum:

$$Z_{w0} = \sqrt{\frac{\mu_0}{\varepsilon_0}} \approx 377\Omega \tag{3.1.16}$$

The amplitudes of the electric and the magnetic fields in air are connected by the relation:

$$E_0 = Z_{w0} H_0 \tag{3.1.17}$$

The Poynting Vector $\vec{S}$ $[W/m^2]$ gives the electromagnetic energy flux density:

$$\vec{S} = \vec{E} \times \vec{H} \tag{3.1.18}$$

In linear, homogenous and isotropic materials far from boundary layers the vectors $\vec{S}$ ($\vec{k}$ is parallel to $\vec{S}$), $\vec{E}$ and $\vec{H}$ are orthogonal (see figure 3.1.1).

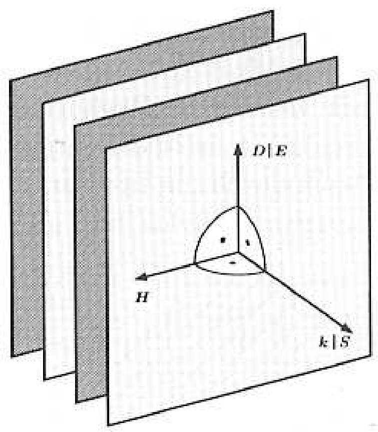

Figure 3.1.1: linear polarized electromagnetic wave, [5]

As the physical aspects of electromagnetic waves stands explained it is useful to figure out some properties in case of the use for LIDAR systems. Electromagnetic waves are not tied to a medium and therefore able to percolate vacuum in comparison to acoustic waves used in sonic detection and ranging (SODAR). The velocity of propagation is several magnitudes higher than the velocity of acoustic waves. Both properties prevent the beam from drifting as occurs in SODAR systems. On the other hand, the effect of the Doppler shift, discussed in chapter 4, is much lower in LIDAR systems demanding a very sensitive detection unit.

3.2 Semiconductor Physics

Semiconductor development in the early 20th century has changed human society rapidly and it does even more today. Many amenities of semiconductors in the context of engineering are derived by the manipulation and use of the space charged region within those conductors. The following chapters contain a brief description of the mechanisms leading to space charged regions.

3.2.1 Quantum Mechanics

The Newtonian mechanics are in general a proper approach to describe the macroscopic behavior of matter, space and time. Energy is, in macroscopic terms, a continuous quantity. If submicroscopic characteristics of particles shall be determined the energy contents are far less and discrete spectrums appear. Quantum mechanics allows the description of these submicroscopic behaviors.

One essential concept of quantum mechanics is the indeterminableness of momentum p $[kgm/s]$ and location Δx $[m]$. They are linked by the equation:

$$\Delta x \cdot \Delta p_x \geq h \tag{3.2.1}$$

This constriction also applies to the detection of energy E_{nrg} and time:

$$\Delta t \cdot \Delta E_{nrg} \geq h \tag{3.2.2}$$

If the initial state of a particle cannot be determined exactly it is not possible to make exact predictions concerning the future behavior of the particle. At this point probabilistic theory is useful to make predictions about particles. The behavior of a submicroscopic particle is specified by a dimensionless wave function $\psi(x,t)$, where the intensity is equal to the probability density of occupation:

$$|\psi(x,t)|^2 = \psi^*(x,t) \cdot \psi(x,t) = P(x,t) \tag{3.2.3}$$

and for 3 dimensions

$$\int\int\int_{-\infty}^{\infty} |\psi|^2 \; dx \; dy \; dz = 1 \tag{3.2.4}$$

Erwin Schrödinger discovered a connection concerning the behavior of the wave function in space and time. In one dimension the relation is as follows:

$$-\frac{h^2}{8\pi^2 m}\frac{\partial^2\psi(x,t)}{\partial x^2}+V(x)\cdot\psi(x,t)=-\frac{h}{2\pi j}\cdot\frac{\partial\psi(x,t)}{\partial t} \tag{3.2.5}$$

where m stands for the mass of the particle and V(x) is represented by the potential energy at the given location x. In some cases stationary solutions of the wave equation can be expected (for example the discrete energy layers of atoms). Therefore a stationary wave function is defined:

$$\psi(x,t)=\psi(x)\cdot e^{-j2\pi\frac{E}{h}t} \tag{3.2.6}$$

leading to the time-independent Schrödinger Equation:

$$-\frac{h^2}{8\pi^2 m}\frac{\partial^2\psi(x)}{\partial x^2}+V(x)\cdot\psi(x)=E_{nrg}\cdot\psi(x) \tag{3.2.7}$$

The solution of this equation needs to meet three requirements:

- the wave function has to be continuous and unique
- the derivations $\partial\psi/\partial x,\ \partial\psi/\partial y\ and\ \partial\psi/\partial z$ have to be continuous
- and as already mentioned in equation 3.2.4 the spatial integral from negative infinity to positive infinity needs to be equal one.

3.2.2 Bohr´s Atomic Model

Figure 3.2.1 shows an infinitely deep one dimensional quantum well. Compared to the potential function within atoms this is just a fictive model. Still it gives insights into fundamental principles of energy layers.

Outside of the well ($x < 0 \quad \& \quad x > x_1$) the potential function V(x) is infinite. As no particle can reach infinite potential the probability for this to occur is zero leading to $\psi(x) = 0$. Within the well, the Schrödinger Equations is reduced to:

$$\frac{\partial^2\psi(x)}{\partial x^2}+\frac{8\pi^2 mE_{nrg}}{h^2}\psi(x)=0 \tag{3.2.8}$$

The mathematical solution of this equation is

$$\psi(x)=a_1 sin\left(\frac{\sqrt{8\pi^2 mE_{nrg}}}{h}x\right)+a_2 cos\left(\frac{\sqrt{8\pi^2 mE_{nrg}}}{h}x\right) \tag{3.2.9}$$

The physical requirements concerning the wave function demand a continuous gradient. This claims that the wave function needs to equal zero at the location $x = 0$ as well

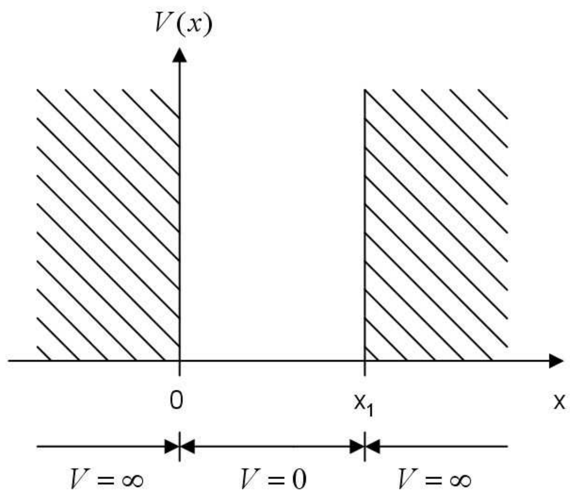

Figure 3.2.1: infinite deep quantum well, [6]

$x = x_1$. As $cos(0) = 1$ the requirement is not met at the location $x = 0$ except for $a_2 = 0$ which leads to no amplitude of cosine functions within the well. The solution of the sinus function is demonstrated below:

$$\psi(x) = a_1 sin\left(\frac{\sqrt{8\pi^2 m E_{nrg}}}{h} x_1\right) = 0 \tag{3.2.10}$$

leads to

$$\frac{\sqrt{8\pi^2 m E_{nrg}}}{h} x_1 = n\pi \tag{3.2.11}$$

and finally

$$\psi(x) = a_1 sin\left(\frac{n\pi x}{x_1}\right) \tag{3.2.12}$$

Equation 3.2.11 shows that the energy level of a particle within the well is discrete. Finally equation 3.2.13 represents the energy levels, fixed due the quantum number n.

$$E_{nrg} = \frac{h^2}{8mx_1^2} n^2 \qquad n = 1, 2, ..., \infty \tag{3.2.13}$$

The amplitude a_1 can be calculated due the standardization given through the equation 3.2.4. In reality the quantum well has neither infinite deepness nor a one dimensional shape. This leads to four quantum numbers defining the energy state of a particle within an atomic layer. Still the energy levels are discrete. Orbitals represent areas with low potential energy leading to a higher likelihood of habitation.

If an electron approaches an atom surrounded within an electric coulomb field, it is opposed to the coulomb force F_c $[N]$. Its potential energy changes according to:

$$E_{pot} = \int\limits_{\infty}^{r} F_C \; dr \tag{3.2.14}$$

If the energy of an electron is defined as

$$E_{nrg} = E_{pot} + E_{kin} \qquad E_{kin} = \frac{m_e v^2}{2} \tag{3.2.15}$$

the kinetic energy within quantum wells has to be discrete leading to discrete velocities. If an electron circles around a positive atomic nucleus it is affected by a centrifugal force F_{cf} $[N]$. Due the positive charged nucleus of an atom the electron is also affected by the coulomb force. To keep the electron within a steady state those forces need to be equal. The forces are defined as

$$F_{cf} = m_e \frac{v^2}{r} \qquad F_C = \frac{e^2}{4\pi\varepsilon_0 r^2} \tag{3.2.16}$$

m_e $[kg]$ represents the mass of an electron and e $[As]$ stands for the negative charge of an electron.

Accordingly to $F_{cf} = F_C$ the radius can be calculated as:

$$r = \frac{e^2}{4\pi\varepsilon_0 m_e v^2} \tag{3.2.17}$$

and thus the discrete velocity leads to a discrete turning radius claimed by Niels Bohr.

3.2.3 Energy Model of Semiconductors

The discrete energy levels within separated atoms are described in section 3.2.2. If the atoms are fixed in a lattice structure the barriers of the quantum well's are small enough to allow new wave function leading to lower energy levels and thus binding atomic forces within the lattice structure.

Figure 3.2.2 shows a wave function and the energy levels of one single and of two hydrogen atoms.

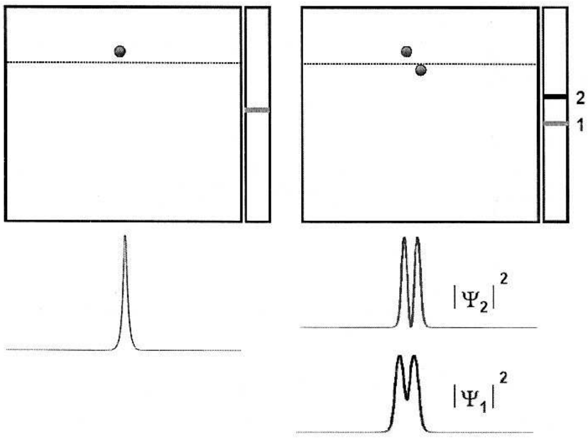

Figure 3.2.2: energy levels and wave functions for one and two hydrogen atoms, [7]

In the case of two atoms the electron can have two stationary states: It can reach a lower energy level by circling both atoms (binding state) or it can stay in the surrounding area of one single atom under the influence of the second atom raising it to a higher energy level (antibinding state). Adding more and more atoms with the same lattice spacing leads to additional energy levels creating an energy band as shown in figure 3.2.3 .

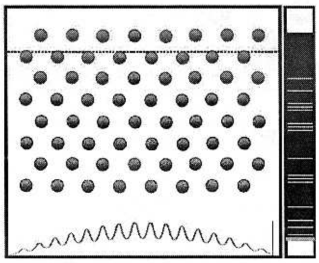

Figure 3.2.3: energy levels and wave function for a symmetric lattice structure, [7]

The continuous energy spectrum is typical for metals. In case of semiconductors the lattice spacing is not the same between every neighboring atom. This leads to far lower energy levels in the binding state and thus an increased energy gap between the binding and the antibinding states. This also explains the mechanical hardness of semi conductors because the binding forces between the atoms are stronger than the ones in metals. Figure 3.2.4 shows an example.

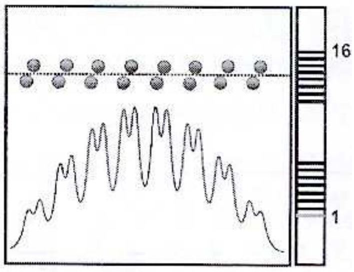

Figure 3.2.4: two dimensional lattice structure of a semiconductor, [7]

The lower energy band is called the valance band, the upper one the conduction band. The energy gap is a crucial attribute of semiconductors. It allows the creation of space charged regions which are explained in the following chapter. To explain the energy model of a specific semiconducting material an analogical three dimensional analysis of the lattice structure is necessary. For the understanding of the fundamental principles of LIDAR systems the one dimensional analysis shown in this chapter is sufficient for the scope of this project.

3.2.4 Hole Pairs, Doping and Direct and Indirect Semiconductors

At very low temperatures the valence band of a semiconductor is filled completely while the conduction band is empty. If the temperatures are higher, electrons can be excited into the conduction band due to collisions with phonons (lattice oscillations) leaving a positive charged hole in the valence band. If a thermodynamic equilibrium exists the density of positive charged holes (p) and negative charged moveable electrons (n) is equal (see equation 3.2.18) allowing intrinsic conduction.

$$p = n = n_i(T) \tag{3.2.18}$$

Due to the doping of semiconductors, the concentration of negative and positive charged holes can be manipulated. Figure 3.2.5 shows an example.

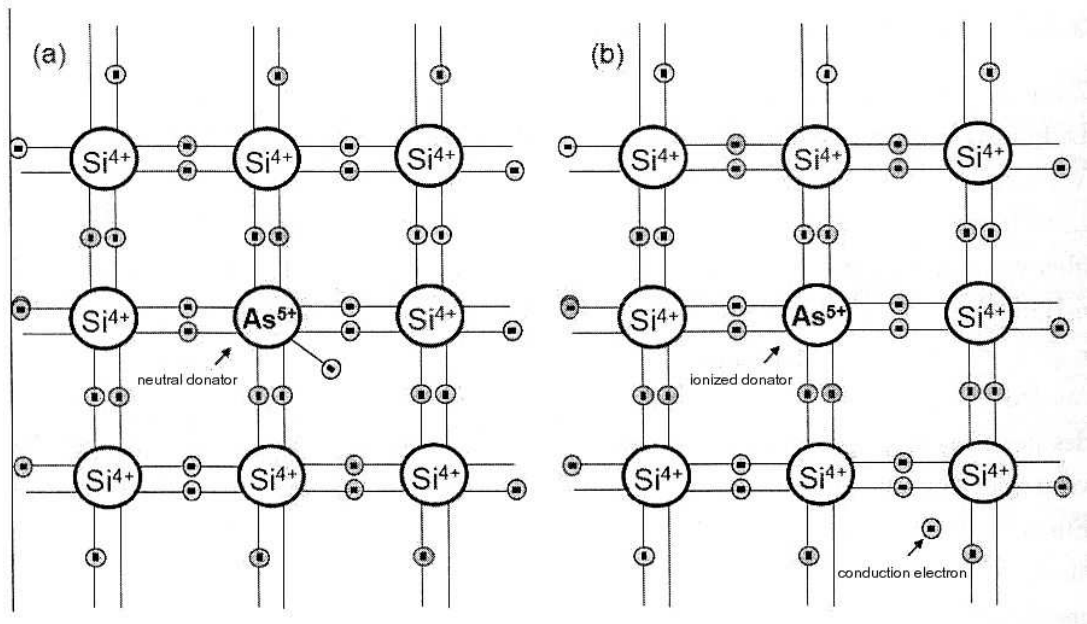

Figure 3.2.5: n- doping, Source: [7]

If an n-doped material comes into contact with a p-doped material the free electrons around the contact area of the n- material are going to recombine with the holes of the p-material leading to a space charged region. The charged region is leading to an electric field along the pn- junction which has several technical meaningful consequences. The ones essential for LIDAR are going to be explained within this chapter. Figure 3.2.6 shows a pn- junction ((a) spatial distribution of donors N_D $[1/cm^3]$ and acceptors N_A $[1/cm^3]$, (b) spatial distribution of electrons and holes, (c) potential distribution $\Phi(x)$ $[V]$ and electric field intensity).

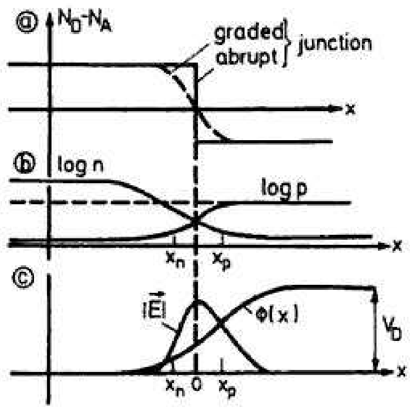

Figure 3.2.6: pn- junction, [8]

Depending on the location of the valence band in relation to the binding band of semiconductors a distinction can be made between direct and indirect semiconductors. In direct semiconductors the maxima of the valence band is right below the minima of the conduct band and the wave number is the same. This is not true for indirect semiconductors. As the occupation probabilities of low energy levels are higher than the one of higher energy level indirect semiconductors like silicium are predestined for the detection of photons due to a high probability of unoccupied free positions in the conduct layer. Direct semiconductors are used as emitters of photons. Figure 3.2.7 shows an example.

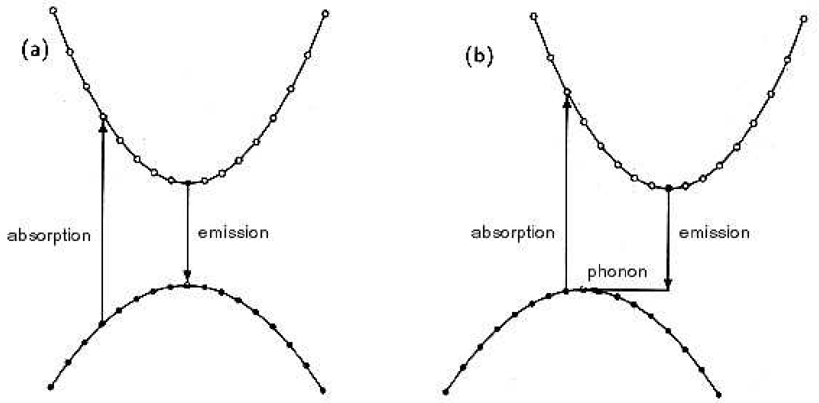

Figure 3.2.7: energy model of a direct and indirect semiconductor, [5]

With an understanding of the process of photon emission and detection, the technical applications of the space charged region can be explored. If hole pairs are created due the absorption of photons the charged region separates these pairs physically and prevents them from recombination. In short, this is the way that photo diodes as well as photovoltaic cells work. LIDAR systems use a photosensitive sensor in order to detect the photons emitted from the LIDAR- Laser.

3.3 LIDAR Systems

Light Detection and Ranging (LIDAR) sytems are operating on electromagnetic waves in order to determine certain parameters about the environment. The wave length of the electromagnetic waves generally range between $250nm$ to about $11\mu m$. Each LIDAR system consists of a transmitter emitting, and a receiver detecting the waves. Figure 3.3.1 shows the principal setup.

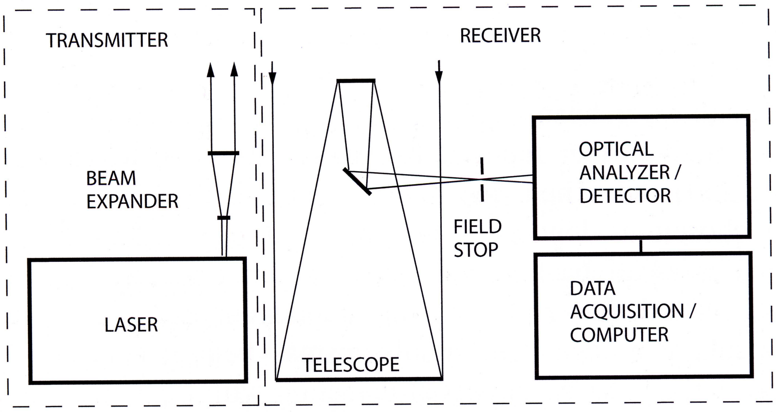

Figure 3.3.1: Principal setup of a lidar system, [9]

The telescope collects the photons that are backscattered from the atmosphere, which are then analyzed by an optical analyzing system. These are different depending on the LIDAR system. Nowadays, with the proper optimized analyzing setup, systems are able to detect trace gasses and their concentration as well as temperature, pressure, humidity, clouds and aerosols.

The geometric arrangement of the emitter and receiver optics determines the degree of signal compression at distances close to the LIDAR. At short distances the spatial length of the laser pulse is longer than the distance between the emitter and the receiver and therefore cannot be imaged completely. This effect also varies with the laser beam diameter, shape and divergence as well as the arrangement of the detector and the receiver. The combination of all these effects results in an individual overlap function.

Signal detection is realized by semiconducting electronic devices like photomultiplier tubes or photodiodes. If the number of photon counts per time interval after emission of the laser pulse is stored the resolved time Δt corresponds to an atmospheric range of $\Delta R = \frac{c\Delta t}{2}$.

3.3.1 LIDAR Equation

A proper mathematical model of Lidar systems consists of the following parameters:

- performance of the system
- transmission losses in the atmosphere
- backscatter coefficient of the atmosphere

- and range dependent geometry factors

The power of the detected signal can be calculated by the LIDAR equation:

$$P(R) = KG(R)\beta(R)T_r(R) \tag{3.3.1}$$

The factor K $[Wm^3]$ summarizes the performance of the system and is called system factor. $G(R)$ $[1/m^2]$ is a range-dependent measurement geometry factor, the term $\beta(R)$ $[1/(m \cdot sr)]$ is called the backscatter coefficient and $T_r(R)$ [1] is a transmission term at a distance R $[m]$. The factors K and $G(R)$ can be manipulated by the experimentalist and are dependent on the Lidar system. The other two, $\beta(R)$ and $T_r(R)$ are in principle unknown and can provide information about the atmosphere.

The system factor K can further be described due the relation:

$$K = P_0 \frac{c\tau}{2} A\eta \tag{3.3.2}$$

P_0 $[W]$ represents the average power output. As a consequence of the convolution of the reflected laser beam the effective pulse length ΔR equals $\frac{c\tau}{2}$ (see figure 3.3.2). Depending on the Lidar system the laser may be pulsed with a certain time period τ $[s]$ or continuous. η [1] describes the systems efficiency and A represents the area of the receiver optics reserved for the detection of backscattered light.

The geometric factor $G(R)$ represents a ratio of the overlap function and the radius to the power of two. The overlap function $O(R)$ [1] allows signal compression at short distances and can be influenced by the experimentalist. Figure 3.3.3 shows an example.

$$G(R) = \frac{O(R)}{R^2} \tag{3.3.3}$$

The quadratic decrease of the geometric factor can be easily reasoned. An isotropic scatterer reflects steadily into an solid angle of 4π (I_s $[W/m^2]$). The overall intensity collected with a telescope I_c $[W/m^2]$ with an area A therefore results in:

$$I_c = \frac{A}{4\pi R^2} I_s \tag{3.3.4}$$

The backscatter coefficient $\beta(R, \lambda)$ describes the amount of light scattered into the backward direction and depends on the atmosphere. If the backscatter coefficient is known, predictions about the atmosphere are possible. In case of Doppler wind LIDARs the constitution of the atmosphere is not a matter of interest. The only requirement the coefficient needs to fulfill is reaching a sufficient high level. N_j describes the concentration

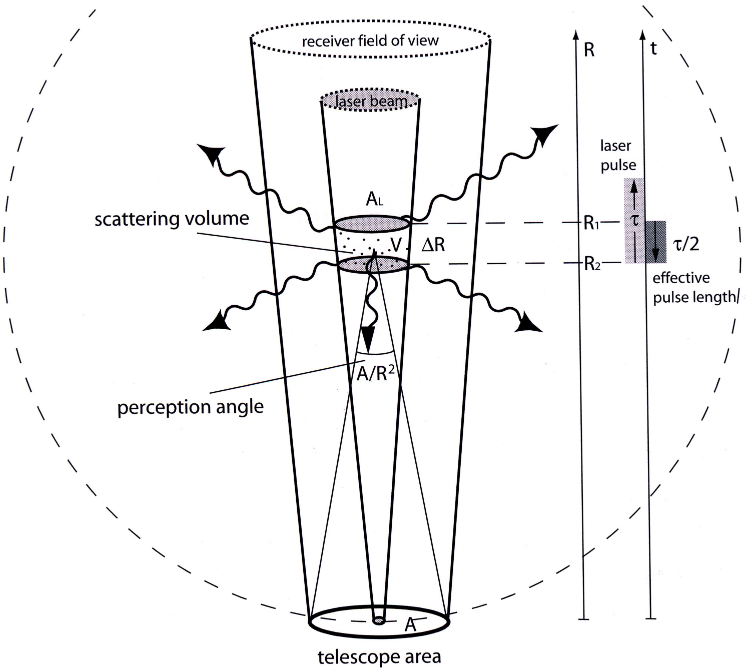

Figure 3.3.2: Illustration of the lidar geometry, [9]

of scattering particles of kind j. The ratio $\partial\sigma_{j,sca}/\partial\Omega$ represents the particles' differential scattering cross section for the backward direction at the wavelength λ.

$$\beta(R,\lambda) = \sum_j N_j(R)\frac{\partial\sigma_{j,sca}}{\partial\Omega}(\pi,\lambda) \tag{3.3.5}$$

If we assume a homogenous medium in which just one kind of particle is scattering the light (which is for this example monochromatic) isotropically the relations can be simplified to $4\pi\beta = N\sigma_{sca}$. If the illuminated volume $V = A_L \cdot c\tau/2$ with the laser beam cross section A_L has the concentration N $[m^3]$ of particles with the scattering cross section σ_{sca} $[m^2/sr]$ an area $A_S = N\sigma_{sca}V$ can be defined which represents the surface of an enclosed ball-shaped shell around the particles. If the volume is illuminated with an intensity I_0 $[W/m^2]$ the intensity of the isotropically scattered light can by calculated by the ratio:

$$\frac{I_S}{I_0} = \frac{A_S}{A_L} = \frac{N\sigma_{sca}c\tau}{2} = \frac{4\pi\beta c\tau}{2} \tag{3.3.6}$$

I_S represents the isotropically scattered overall intensity. As the area of the receiving telescope covers just a part of the solid angle the collected intensity can be calculated by

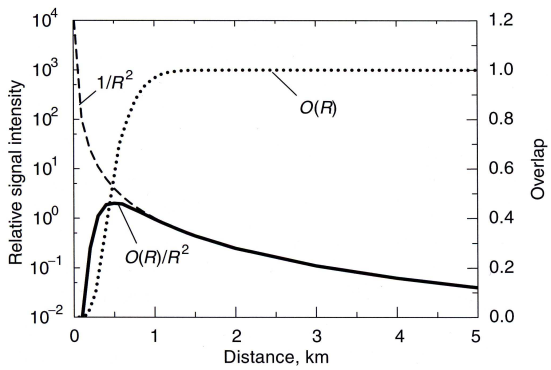

Figure 3.3.3: Influence of the overlap function on the signal dynamics, [9]

using the equation 3.3.4:

$$I_c = \frac{A\beta c\tau}{2R^2} I_0 \tag{3.3.7}$$

The scattering process in the atmosphere is caused by air molecules (mainly nitrogen and oxygen) and particulate matter. The backscatter coefficient can be written as:

$$\beta(R, \lambda) = \beta_{mol}(R, \lambda) + \beta_{aer}(R, \lambda) \tag{3.3.8}$$

Particles have a great variety of scatterers like liquid and solid air-pollution particles. These may consist of sulfates, soot and organic compounds, mineral-dust and sea-salt particles, pollen, clouds and rain droplets as well as ice crystals to mention a few.

The last parameter remained unexplained had been the the transmission term $T(R)$. Actually it is also a function of the wavelength λ and can be calculated by:

$$T_r(R, \lambda) = exp\left[-2\int_0^R \alpha(r, \lambda)dr\right] \tag{3.3.9}$$

α $[1/m]$ is called extinction coefficient, the factor 2 derives from the two-way transmission path. The transmission term has always values between 0 and 1.
Extinction may occur due scattering and/or absorption of light by molecules and particles. Therefore the extinction coefficient consists of four terms:

$$\alpha(R, \lambda) = \alpha_{mol,sca}(R, \lambda) + \alpha_{mol,abs}(R, \lambda) + \alpha_{aer,sca}(R, \lambda) + \alpha_{aer,abs}(R, \lambda) \tag{3.3.10}$$

while the extinction coefficient can be calculated by

$$\alpha(R, \lambda) = \sum_j N_j(R)\sigma_{j,ext}(\lambda) \tag{3.3.11}$$

and the extinction cross is defined due:

$$\sigma_{ext}(\lambda) = \sigma_{sca}(\lambda) + \sigma_{abs}(\lambda) \tag{3.3.12}$$

Inserting these equations into equation 3.3.1 leads to the final lidar equation:

$$P(R,\lambda) = P_0 \frac{c\tau}{2} A\eta \frac{O(R)}{R^2} \beta(R,\lambda) exp\left[-2\int_0^R \alpha(r,\lambda)dr\right] \tag{3.3.13}$$

In comparison to equation 3.3.1 the dependence of the wavelength can be seen clearly.

3.3.2 LIDAR Techniques

The LIDAR equation was described in chapter 3.3.1. The knowledge of the relations of received power, system parameters and the composition of the atmosphere allows the use of LIDAR techniques for the determination of several atmospheric parameters. In this chapter basic LIDAR techniques and its applications are explained briefly.

Elastic-backscatter LIDAR

In case of elastic scattering the wavelength of the reflected signal remains unchanged. Elastic scattering can be caused by molecules and aerosols and shows a strong wavelength dependence as well as a dependence on the size of the aerosols. Therefore elastic-backscatter can be used to obtain information on size and other parameters of atmospheric aerosol particles.

Raman LIDAR

Raman scattering describes in general an inelastic scattering process. The wavelength of the scattered changes due energy absorption or emission of the energy level of the reflecting molecule. As the population of energy levels follows Boltzmann's distribution law, an analysis of the intensity distribution of the reflected signal allows to determine temperature profiles. Raman LIDAR technique is also applied to the measurement of water vapor.

Differential-absorption LIDAR

The strong wavelength dependence of the backscatter coefficient of different gases makes a detection possible. The sensitivity of systems can be further increased when two specific wavelengths are emitted. The comparison of the reflected signals allows the determination of the concentration of gas molecules or atoms.

Fluorescence LIDAR

If the energy of the emitted photons coincides with the energy of a transition within an atom, electrons can be raised to a higher energy state. The electron needs not to fall back to the prior energy state but can also end up on another one. Therefore the reemission of light can occur at longer wavelengths. The cross sections for resonance scattering are extremely high resulting in strong LIDAR signals. This allows the detection of very low atom concentrations.

Doppler LIDAR

Doppler LIDARs are using the Doppler effect to determine the speed of matter and/or objects. Doppler wind LIDARs are especially designed for the determination of wind speed which leads to very specific requirements. The main part of this thesis, the determination of the power curve, was done by measuring the wind velocity with a Doppler LIDAR. A detailed description of the Doppler wind LIDAR follows in chapter **??**.

Chapter 4

Doppler Wind LIDAR

The measurement of wind speeds in the field of wind energy is still dominated by the use of conventional cup anemometers, which are usually mounted on a nacelle or on stand alone measuring masts. Since hub heights of wind turbines now often exceeds 90m, the traditional mast-mounted anemometer has become an expensive and logistically complex affair. Anemometers can only determine the velocity transverse to its axis of rotation and have a moment of inertia due their mass. Still the use of two anemometers allows a three dimensional determination of the wind speed. One disadvantage is the punctual measuring point of each anemometer. Each measuring point represents a dot within space. The air surrounding the anemometer may have the same speed at close distances, but a volume measurement generally is not possible. This is not true for Doppler Wind LIDARs. This chapter contains a basic description of Doppler Wind LIDARs. Figure 4 gives an overview of the mentioned LIDAR systems. The topics contained in the grey fields are of high relevance for the practical application of Doppler wind LIDAR systems.

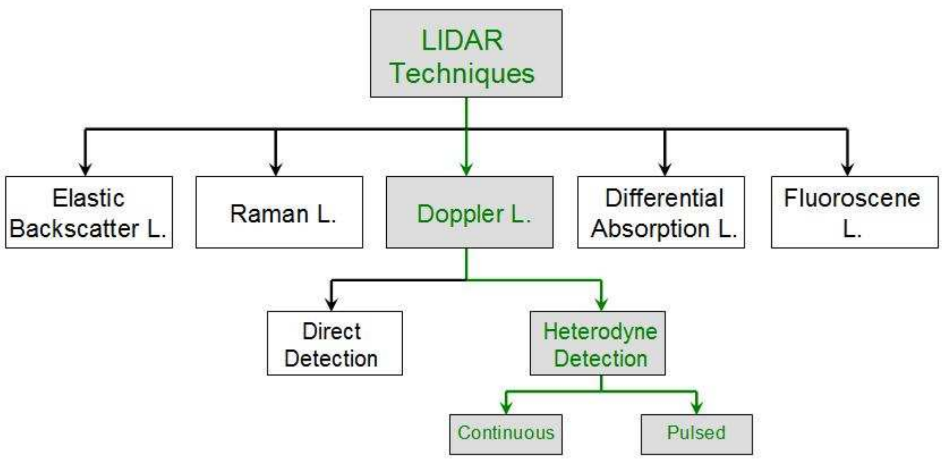

Figure 4: Overview of LIDAR systems, [10]

4.1 Doppler Effect

The Doppler effect was first discovered in the field of acoustics, but it is true for every type of propagated wave. If a source is emitting a wave with a frequency f_0 (may it be air pressure in case of acoustics, electromagnetic field intensities in case of electromagnetic waves or other mechanical waves) spreading with the speed c $[m/s]$, and the relative speed along the line is v, then, the frequency, received by an observer, is:

$$f = f_0 \left(1 + \frac{v}{c}\right) \tag{4.1.1}$$

If the wave is reflected by an obstacle moving with the relative speed v the Doppler effect acts on two ways. The frequency of the wave reflected back to the emitter therefore can be calculated by:

$$f = f_0 \left(1 + \frac{2v}{c}\right) \tag{4.1.2}$$

The propagation speed of light depends on the medium and is defined by the Maxwell equations in connection with the constitutive relations. Together they are leading to the Maxwell Relation, in vacuum $c_o := \frac{1}{\sqrt{\varepsilon_0 \mu_0}}$, as already mentioned in chapter 3.1.1. Within the medium air, the propagation speed of light is approximately c_o. It can be determined as:

$$c_o = \frac{1}{\sqrt{\varepsilon_0 \mu_0}} = 2.998 \cdot 10^8 m/s \tag{4.1.3}$$

Detectable /footnoteUsing commercial Doppler wind LIDARs velocities of air masses in the atmosphere range between 0.1 to 100 m/s. Compared to the velocity of light the movement of air mass is extremely slow, leading to a very low v/c ratio. It ranges between 3 parts in 10^{10} to 3 parts in 10^7. Therefore sophisticated detection techniques are necessary, as described in chapter 4.2.

As already mentioned in chapter 3.3.2 atoms, molecules and aerosols contribute to the backscattered signal. The mass of an aerosol exceeds the mass of atoms and molecules by far. Therefore the relative shift of their velocity distribution due to temperature is rather small. For atoms and molecules the shift often exceeds the wind speed leading to a large reflecting spectrum. Figure 4.1.1 gives an example (the peak due the presence of aerosols can be clearly seen, I_c represents the intensity of the backscattered signal, LOS is an acronym for line of sight).

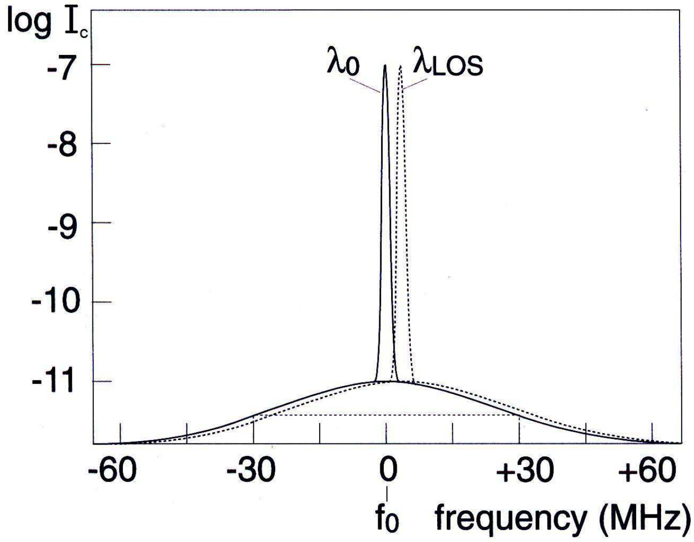

Figure 4.1.1: Doppler shift of the backscattered photons, [9]

4.2 Detection Techniques

The very low ratio of v/c leads to extremely low frequency shifts. Therefore highly sensitive detection techniques are necessary. Depending on the main contributors to the backscattering effect (atoms and molecules or aerosols) the spectra of the scattered signal shows a significant peak (in case of aerosols) or has the shape of a gaussian curve. Figure 4.2.1 shows the return spectrum of a spaceborne LIDAR emitting waves from the outside into the atmosphere. Despite the quadratic decrease of the wave intensity with distance, the number of detected photons is significant higher for the lower atmospheric layer (3km). This is reasoned by a higher density of air as well as a higher number of aerosols, causing the spike in the spectrum. Independent of the main contributor of the backscattering effect, the movement of air mass will cause a Doppler shift. This shift is obvious for aerosols. In the case of atoms and molecules the whole gaussian curve shifts similarly, but the detection is more difficult due the broadness of the spectrum.

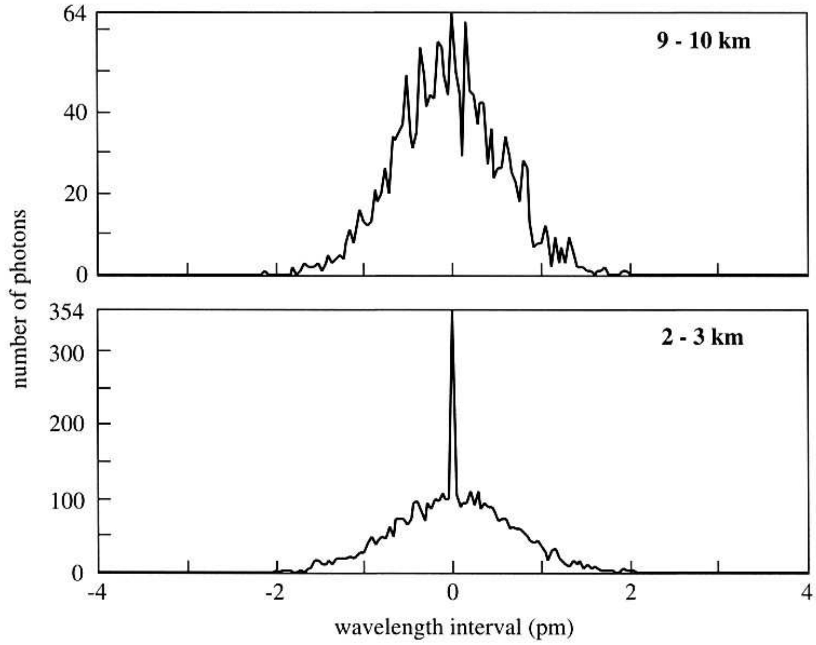

Figure 4.2.1: Return spectra for a spaceborne LIDAR operating at a wavelength of 355nm. Spectra from a 2 to 3 (from the ground) and 9 to 10 km height respectively, [9]

4.2.1 Direct Detection

In case of Direct Detection, the signal is matched with passive methods in order to obtain the velocity of the wind. The matching process can involve the use of high-dispersion multichannel spectrometers as well as several narrow-band optical filters. If atomic and molecular scattering is dominant, the expected gaussian curve may be calculated in order to use the optimum filter configuration. Therefore parameters like temperature and the contribution of aerosol scattering should be known. The LIDAR system used in this project is based upon heterodyne detection. Its description follows in the next chapter.

4.2.2 Heterodyne Detection

Two commercial Doppler wind LIDAR systems (further described in chapter 5.2) are now available, both using heterodyne detection (also known as coherent detection). In heterodyne detection the backscattered signal is mixed with the radiation of a local optical oscillator. This mixing causes a multiplication of the time functions. A multiplication in time, $signal_1(t) \cdot signal_2(t)$, equals a convolution of the spectrums $signal_1(\omega) * signal_2(\omega)$.

The Fourier transformation of a sinus function in time with the amplitude A is:

$$\mathbf{FT}\left[Asin(\omega_1 t)\right] = F(j\omega) = \int_{-\infty}^{\infty} Asin(\omega_1 t)e^{j\omega t}\, dt = j\pi A[-\delta(\omega-\omega_1)+\delta(\omega+\omega_1)] \quad (4.2.1)$$

Whereas the dirac impulse δ is defined by:

$$\int_{-\infty}^{\infty} \delta(\omega)\, d\omega = 1 \quad whereas \quad \delta(0)=\infty \quad and \quad \delta(\omega)=0 \quad while \quad \omega \neq 0 \qquad (4.2.2)$$

The convolution is calculated by:

$$s_1(\omega) * s_2(\omega) = \int_{-\infty}^{\infty} s_1(\Phi)s_2(\omega-\Phi)\, d\Phi \qquad (4.2.3)$$

Φ $[rad/s]$ represents a control variable. The oscillator phase is fixed by a locked loop to the phase of the emitting laser. If two sinus functions with the same phase and frequency are folded, the outcome is a signal with a constant component and a component with a doubled frequency ($A_{new}[\delta(\omega)+\delta(\omega-2\omega_1)]$ which equals for $A_{new}=1$ the time function: $\frac{1}{2}+cos(2\omega_1 t)$).

As already mentioned, the frequency shift of the backscattered signal is very low. If the local oscillator is also mixed with the backscattered signal the convolution leads to two frequency components: A very low frequency component and to a component with approximately a doubled frequency. This low frequency component is easy to measure, and therefore is the source for further computational algorithms. The frequency of this signal is proportional to the Doppler shift, therefore the computing algorithms are easily implemented. Figure 4.2.2 shows the principle design of a heterodyne detection Doppler LIDAR. TE represents the transmitting laser, LO stands for local optical oscillator, D1 and D2 are two heterodyne detectors and LL represents the locked loop. The right part of the figure shows a transmitter-receiver telescope. The output of D1 and D2 is computed in order to determine the wind velocity.

Compared to other LIDAR systems, heterodyne detection LIDARs are unique because they require the following:

- a pulsed, narrow-frequency, ultrastable high-power laser,

- a second narrow-frequency laser usually referred to as a local oscillator
- a fast detector in which the return and LO signals are mixed
- a second fast detector in which the transmitted and LO signals are mixed (the so-called pulse monitor)
- the presence of aerosol particles

Heterodyne detection LIDAR relies on the aerosol scattering with very narrow Doppler broadening. Therefore it applies only to atmospheric regions with sufficient amount of aerosols. Molecular scattering has a Doppler broadening not suitable for heterodyne detection. Heterodyne detection has become commercial for Doppler wind LIDARs. The laser emitting systems existing on the market are somehow different. The following chapter gives an overview of the systems and their differences.

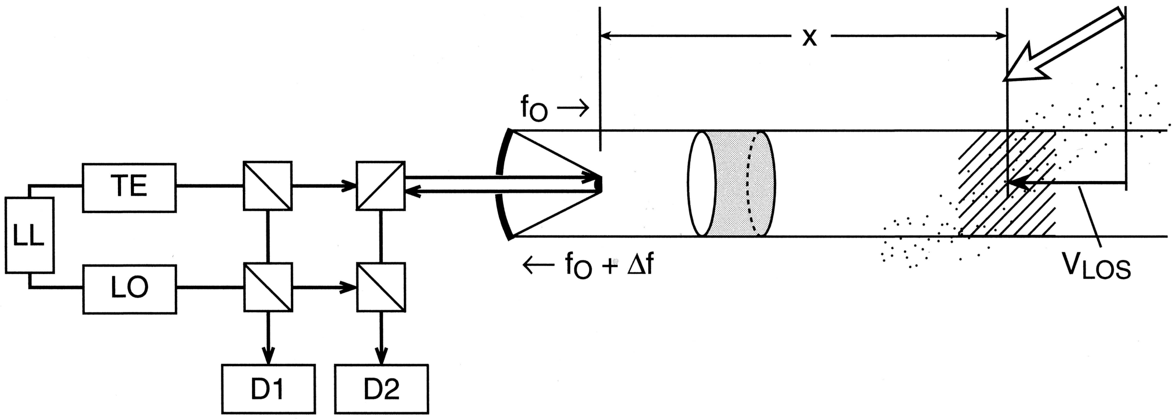

Figure 4.2.2: Principle design of a heterodyne detection doppler LIDAR, [9]

4.3 Emitting Systems

The basic concept of the emission of electromagnetic waves by semiconductor appliances as lasers has been described in chapter 3.2 and 3.3. Figure 3.3.2 showed a laser beam with a spatial limited laser pulse length, assuming a pulsed LIDAR system. But pulsed lasers are not the only way to obtain information about distance and probe depth. As already mentioned two different commercial Doppler wind LIDARs are available on the market. Both of them are using heterodyne detection, but one system is based upon continuous waves while the other emits pulsed waves. This leads to different concepts for the calculation of depth range and distance.

4.3.1 Continuous-Wave Doppler LIDAR

Continuous-wave (CW) Doppler LIDARs are permanently emitting electromagnetic waves. Therefore a pulse length cannot be specified. The continuous emission of photons would cause permanent backscattering from the illuminated solid angle allowing the determination of aerosol concentration as a function of signal intensity, but not the determination of the wind velocity in a certain volume. In order to obtain spacial information, CW LIDAR systems can be focused by purely geometric means. If the detection system (with the the detector area A represented by the telescope diameter and the wavelength λ) is focused to distance x, then approximately half of the backscattered signal has been reflected in a depth range of:

$$\Delta x = \frac{4x^2\lambda}{A} \tag{4.3.1}$$

Thus the quadratic decrease of the depth range by distance limits CW Doppler LIDARs to short range measurements up to several 100m, depending on the wavelength used and the accuracy demanded. Further, CW Doppler LIDARs need to be focused on a specific distance. Simultaneous measurement at several heights are not possible, since the measurement takes place sequentially.

4.3.2 Pulsed Doppler LIDAR

Pulsed Doppler LIDARs are emitting pulsed electromagnetic waves. The laser is emitting photons for a certain time (pulse length τ). During this time the wave spreads in space within the illuminated volume with the speed $c = 2.998 \cdot 10^8 m/s$. This leads to a spatial pulse length of:

$$\Delta x = c\tau \tag{4.3.2}$$

Therefore the time τ is crucial for the spatial resolution of a pulsed Doppler LIDAR system. The advantages of this system are:

- the resolution and the accuracy of the system remains the same at any height
- the system needs not to be focused on a specific height
- and can therefore perform simultaneous measurements at different heights

4.4 Scan Techniques

The Doppler shift of a reflected signal always represents the velocity of the scattering particle in the line of sight. To obtain a three dimensional velocity vector, data of at least three independent lines of sight are necessary. Most Doppler wind LIDARs are using one punctual laser. This excludes the possibility of local crossing the laser beams in order to determine the speed in a certain point in space. Three different lines of sight are leading in this case to a volume measurement. Therefore the resulting velocities are always connected with volumes. The assumption of continuous wind speeds within this volume is essential for the calculation. In case of turbulence within the volume the requirements of the mathematical algorithms are not met, affecting the accuracy of the measurement. If turbulence is detected, some LIDAR systems offer the option to change the scanning cone angle.

In practice two scan techniques have evolved. The Velocity-Azimuth Display Technique (VAD) is a conical scan method whereas the Doppler Beam Swinging Technique (DBS) derives its information by the combination of single lines of sight. Both techniques are described in the following chapters.

4.4.1 Velocity-Azimuth Display

In case of velocity-azimuth display (VAD) the axis of the laser beam has a tilt in relation to the vertical axis of the LIDAR system. The laser beam is circling, forming a conical scan. Depending on the received direction and time, the backscattered electromagnetic waves are detected and evaluated. The laser circles with a certain speed and the detection unit determines the Doppler shift with a certain resolution in accuracy and time. Figure 4.4.1 shows an example for VAD and DBS techniques. The turning of the laser beam leads to different Doppler shifts, depending on the line of sight. Figure 4.4.2 for instance shows a velocity scan using the VAD technique. The offset, a $[m/s]$, represents the vertical wind speed, whereas the θ_{max} $[rad]$ determines the horizontal wind direction. The value of b $[m/s]$ seen in figure 4.4.2 allows to calculate the value of the horizontal wind speed. The three dimensional wind vector can be calculated by:

$$\vec{v} = -b\frac{sin\theta_{max}}{cos\varphi}\vec{e}_x - b\frac{cos\theta_{max}}{cos\varphi}\vec{e}_y - a\frac{1}{sin\varphi}\vec{e}_z \tag{4.4.1}$$

The vectors e_x [1], e_y [1] and e_z [1] represent an orthonormal coordinate basis with arbitrary origin. e_z is pointing in the vertical direction, e_x to east and e_y to south. The sine-wave fit seen in figure 4.4.2 has to be done for each height interval. In case of non-moving (mostly ground based) LIDAR systems, no shift needs to be removed in the calculation and the data can be used directly to determine the actual wind speed.

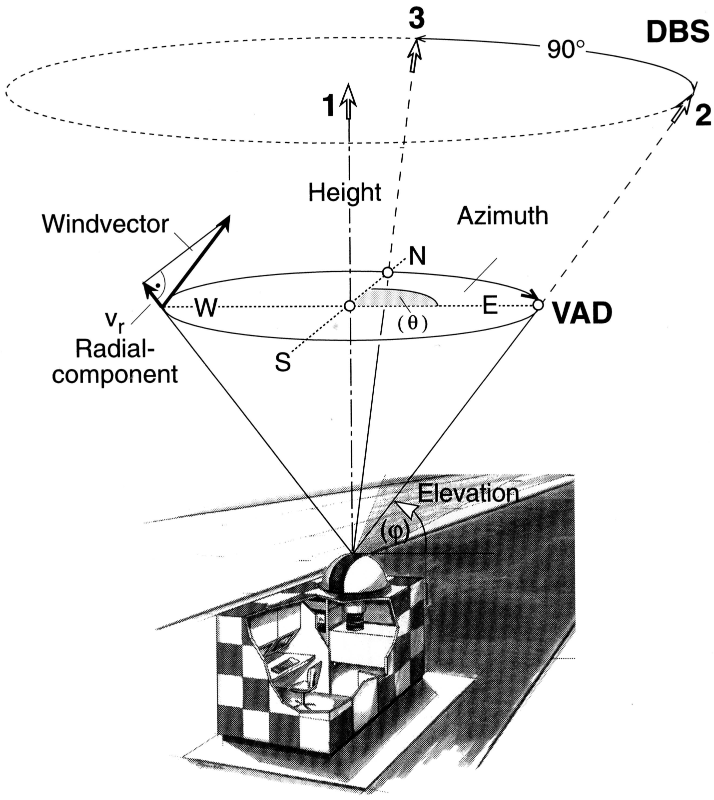

Figure 4.4.1: Schematic of the scan technique of a Doppler LIDAR. Lower part: VAD scan, upper part: DBS scan, [9]

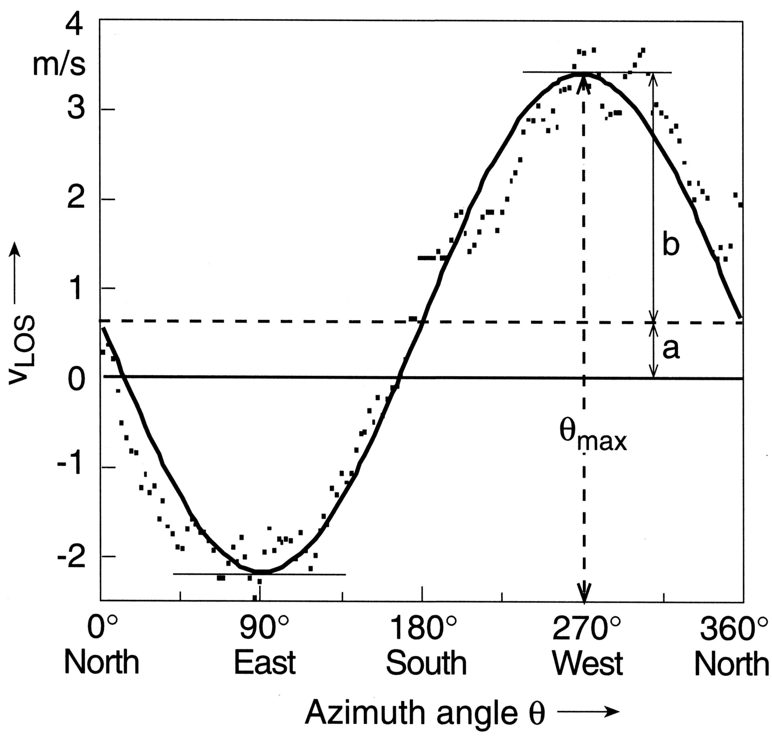

Figure 4.4.2: Example of sine fitting of the radial wind velocity simulated with the use of the VAD technique, [9]

4.4.2 Doppler Beam Swinging

The Doppler beam swinging technique does not make use of a conical scan pattern. It scans in at least three different lines of sight and allows in this way the calculation of the wind vector. The arrangement of the scanning directions can be various. For example, four measurements at azimuth-angle intervals of 90° or three at 120°, or two at 90° in addition to one vertical scanner are possible. The mathematical algorithm needs to match the actual emitting and detecting systems. Due the lower number of measuring directions the DBS technique is faster and simpler from both with respect to hardware and the data evaluation algorithm. On the other hand it lacks on the goodness-of-fit information used to determine the reliability of the results. Figure 4.4.3 shows a schematic of the scanning configuration of the windcube LIDAR.

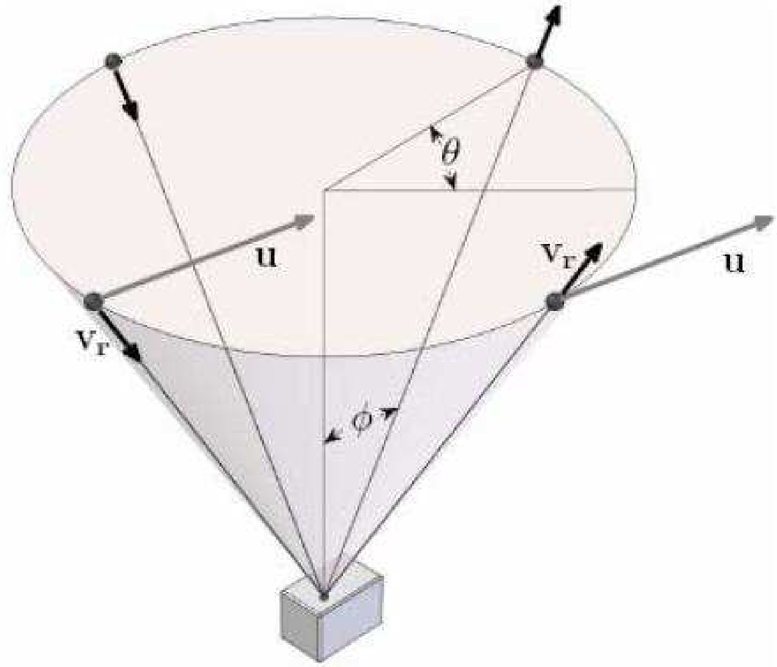

Figure 4.4.3: Scanning configuration of the windcube LIDAR, [11]

4.4.3 Comparison of Doppler LIDAR and Doppler SODAR

SODAR stands for sonic detection and ranging. Doppler SODARs are emitting acoustic waves instead of electromagnetic waves. This leads to several differences between LIDARs and SODARs. Acoustic waves are tied to a medium in contrast to electromagnetic waves which are not. The sonic speed in air (with a temperature of 20°C and a pressure of 1013hPa) is approximately $c = 343m/s$ leading to significant greater ratio of wind speed v to sonic speed c. This causes stronger Doppler shifts. On the other hand the slow velocity does not allow fast scan rates at greater distance since the acoustic waves need a rather long time to travel through the medium. For instance, the determination of the wind speed in a distance of 100m takes at least $2 \cdot \frac{100m}{343m/s} = 0.58309s$. During this time the acoustic wave (which is also backscattered by aerosols as described for LIDARs) is exposed to the movement of the medium itself. Beam drift decreases the accuracy of SODAR systems. SODAR systems are sending the acoustic waves by several speakers based upon piezo elements. This represents a mechanical part which is prone to abrasion. Frequent maintenance of the speaker system is necessary. Normally SODAR systems are sending the waves with a frequency of several kHz which is clearly audibly to listeners. Finally, the system is also sensitive to background noise. On the other hand the SODAR technology is highly sophisticated, cheap and a good complement to small and easy installed measuring masts, often providing sufficient data.

The technology associated with Doppler wind LIDARs is rather young and the accuracy of these systems is already extending the accuracy of SODARs. This gap may further increase in future. The prices of LIDAR systems are very high, but are always decreasing due to the economics of scales. In the authors point of view the actual advantages of SODAR systems, meaning low prices, moderate accuracy and high maturity, will loose substance in future. LIDAR systems have strong physical advantages. Technological development will increase either the maturity and the accuracy of the systems while offering reasonable low prices in future.

Chapter 5

Project Data

The theoretical discussion and description of wind turbine generators and LIDAR systems has been the core of the previous chapters. Wind utilization in general, wind power, electromagnetic waves, quantum mechanics and semiconductor physics as well as different LIDAR systems has been mentioned. The following chapters deal with the practical contents of this thesis. It involved the choice of a fitting LIDAR system as well as an adequate location on the project site in order to measure the power curve. Data had to be collected, filtered, combined and processed. Since there is no standard set yet for the measurement of power curves by using remote sensing technology, different approaches have been tested. Still, wherever possible, the approach was identical or close to the one which is defined for cup anemometers within IEC 61400-12-1.

The project site was located in Bruck, Austria, and comprised five wind turbines owned and operated by VERBUND Renewable Power GmbH. At first, research needed to be done in order to determine the state of the art in remote sensing technology. As already mentioned SODAR, CW- LIDARs and Pulsed- LIDARs are possible approaches allowing remote sensing of wind speeds. Several wind consultants had been contacted and assessed. The swiss consultant "Meteotest" was charged to run the series of measurement. The measurement elapsed from the 07th of July up to the 30th of September in order to collect sufficing data to evaluate the technology and to calculate the measured power curve. Additionally, a cup anemometer had been mounted on the nacelle of the selected WTG in order to complement the remote sensing data. The analysis of data gained by the anemometer is not contained in this thesis.

5.1 Project Site: Windpark Bruck

Bruck is a town in Lower Austria, close to the northern border of Burgenland and Lower Austria. The favorable wind conditions in this area have resulted in a high density of wind farms. One of those farms is owned by VERBUND Renewable Power GmbH. It is located at the geographic coordinates 48°01'48.98"N, 16°43'26.48"E on a height of 175m above sea level. The main wind direction comes from west-northwest. The Doppler wind LIDAR was placed next to the WTG number four. Figure 5.1.1 shows a map of the project site and the LIDAR arrangement.

Figure 5.1.1: project site: Bruck an der Leitha, [12]

5.1.1 Wind Turbine Generators in Bruck

The wind park Bruck was comissioned in the year 2000 and equipped with 5 WTGs by the manufacturer Enercon (type E-66 / 18.70). The WTG has a rated power of 1800 kW. It is based upon a directly rotor-driven variable-speed synchronous generator with a frequency inverter. The power is regulated by pitching and yawing. A detailed description of the technical data can be seen in figure 5.1.2.

Data Sheet Enercon E-66 / 18.70	
operating data	
rated capacity	1800 kW
rotor diameter	70m
hub height	65m
converter concept:	gearless, variable speed, variable blade pitch
remote monitoring system:	enercon scada
direction of rotation:	clockwise
number of blades:	3
sound power level (10 m/s):	103 dB
cut-in wind speed	2 m/s
cut-out wind speed	25 m/s
generator	
concept:	direct driven enercon synchronous ring generator
frequency:	variable
voltage:	790 V
current:	2080 A
number of poles:	72
rotation speed:	8-22.5 rpm
diameter:	5m
generator weight:	50.6 t
grid feeding:	enercon inverter
rotor	
diameter:	70m
swept area:	3848 m²
rotor blade mass:	4t
material	glass fiber reinforced plastic and epoxy
tip speed:	100-300 km/h
nacelle	
maximum diameter:	5.4m
length:	11.6m
gross weight:	100t
nacelle weight:	27t
hub weight:	19.3t
tower	
height:	63m
tower weight:	134t
lower diameter:	4.4m
upper diameter:	2.2m
tower segments:	5
foundation	
diameter:	12.5m
depth:	2.5m
involved steel:	15.5t
involved concrete:	150 m³

Figure 5.1.2: data sheet: Enercon E66 / 18.70, [13]

As already mentioned the power curve is the essential characteristic of each WTG. The proper design of a wind park requires information about the wind distribution and the power curves of different WTGs in order to find best fitting solutions. Figure 5.1.3 shows the warranted power curve of the WTG model enercon E66 / 18.70:

wind speed (m/s)	power (kW)
1	0
2	0
3	2
4	34
5	101
6	195
7	333
8	501
9	722
10	990
11	1318
12	1629
13	1798
14	1820
15	1820
16	1820
17	1820
18	1820
19	1820
20	1820
21	1820
22	1820
23	1820
24	1820
25	1820

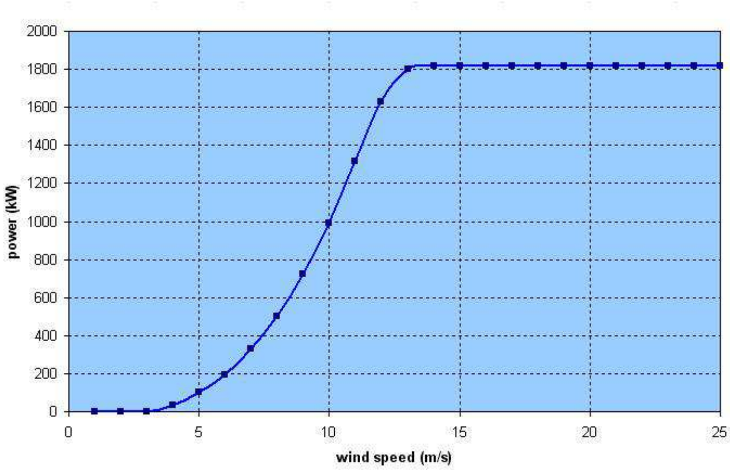

Figure 5.1.3: warranted power curve, [13]

5.2 Selection of Remote Sensing Equipment

5.2.1 Market Research

Several well known wind consultants had been contacted in order to determine wether they offer LIDAR measurements or not. After one month of market research in January 2010 six consultants had been asked for concrete offers for a series of measurement lasting from one to three months during the summer of 2010.

The offers had been compared using the following criteria:

- laser technology (cw or pulsed)
- external calibration before the start of the series of measurement
- assembling and reshipment
- safety and insurance
- final evaluation
- validation of the power curve
- references
- project costs

The offered LIDAR appliances had been a product from the British manufacturer "Naturalpower" called ZephIR (CW) and a product from the French manufacturer "Leosphere" called Windcube (pulsed). Further descriptions of these two Doppler wind LIDARs follows in chapter 5.3 and chapter 5.4. The offers differed strongly in terms of costs as well as content. A comparison can be seen in figure 5.2.1. For confidentiality the exact prices and consultant names are not mentioned. Two of the best offers made it into the short list and were asked to specify their offers (see figure 5.2.2). Finally, in the beginning of April, the Swiss wind consultant "Meteotest" was assigned to run the series of measurement.

	wind consultants				
	A	B	C	D	E
price 1 month		high	low	low	
price 2 months		high		low	
price 3 months	low	high		low	medium
LIDAR system	Windcube	Windcube	ZephIR	Windcube	ZephIR
Callibration before measurement	No	Yes	No	Yes	Yes
assembling and reshipment	Yes	Yes	Yes	Yes	Yes
safety and insurance	Yes	Yes	maybe Yes	Yes	No
final evaluation	Yes	Yes	Yes	Yes	Yes
valdidation of the power curve	No	maybe Yes	Yes	No	Yes
references	Yes	Yes	No	Yes	Yes

Figure 5.2.1: consultants offers

	A	D
price 1 month		low
price 2 months	medium	low
price 3 months	medium	low
LIDAR system	Windcube	Windcube
Callibration before measurement	No	No
assembling and reshipment	Yes	Yes
safety and insurance	Yes	Yes
final evaluation	Yes	Yes
valdidation of the power curve	No	No
references	Yes	Yes

Figure 5.2.2: short list

5.3 ZephIR

The continuous wave Doppler LIDAR "ZephIR" is manufactured by a British company called Naturalpower. ZephIR emits and detects electromagnetic waves with a wavelength of 1575nm. As continuous wave LIDARs are constantly emitting electromagnetic waves, the telescope needs to be focused for the determination of the measurement height. The beam is rotating in circles, taking 150 measurements in approximately three seconds per measurement height. The Doppler shift is detected by using heterodyne detection described in chapter 4.2.2, the scanning technique is VAD (see chapter 4.4.2). Figure 5.3.1 shows a picture of the ZephIR.

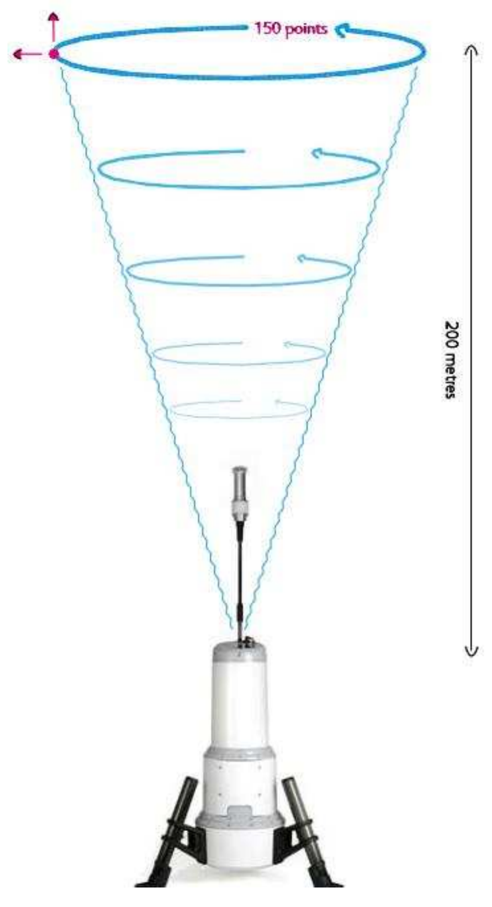

Figure 5.3.1: wind doppler LIDAR ZephIR by Naturalpower, [14]

The general specifications can be seen in figure 5.3.2.

GENERAL SPECIFICATIONS	
SYSTEM DIMENSIONS: OPTICS POD ELECTRONICS POD BATTERY POD	 345mm dia. x 660mm length 450mm dia. x 390mm length 550mm dia. x 290mm length
SYSTEM WEIGHT: OPTICS POD ELECTRONICS POD BATTERY POD BATTERIES (removable) TRIPOD MET MAST TOTAL	 28kg 24kg 20kg 44kg 14kg 4kg 134kg
OPERATING TEMPERATURES	-25ºC to +40ºC
SYSTEM POWER REQUIREMENTS	28v DC @ 100W continuous @ 0ºC to 25ºC
MAINS POWER SUPPLY: INPUT RANGE OUTPUT	 100 - 240V a.c. 50/60Hz 300VA 28V d.c. 9A max.
SAFETY ACCREDITATION	CE marked meeting all the essential requirements of all applicable EU directives

SYSTEM SPECIFICATIONS	
MEASUREMENT RANGE: Min. height Max. height	 11m 200m
Max. WIND SPEED	$70ms^{-1}$
Min. WIND SPEED	$2ms^{-1}$
LASER CLASSIFICATION	CLASS 1 LASER
LASER WAVELENGTH	1575nm
DATA STORAGE	3 days RAW data, 365 days wind data
DATA OUTPUT	Wind data (1s averages) User defined wind speed averages (i.e. 1, 5, 10 minutes) Temperature Pressure Humidity
FOCUS HEIGHTS	5 user programmable heights up to 200m
PROBE DEPTH: @ 11 metres @ 20 metres @ 40 metres @ 110 metres	 +/- 0.12 metres +/- 0.4 metres +/- 1.6 metres +/- 12.3 metres

Figure 5.3.2: general specifications: ZephIR, [14]

5.4 Windcube

The Doppler wind LIDAR "Windcube" is manufactured by the French company Leosphere. It is a pulsed waved Doppler wind LIDAR based uppon heterodyne detection and DBS scanning (see chapter 4.2.2 and 4.4.2, figure 5.4.1 gives an example). Windcube is used by several wind consultants. It dominates the market together with the CW system ZephIR. In terms of accuracy and reliability both systems seem to be competitive despite the different technology. One advantage of the pulsed LIDAR systems is that the accuracy is independent of the measurement height. Detailed specifications of the windcube can be seen in figure 5.4.2.

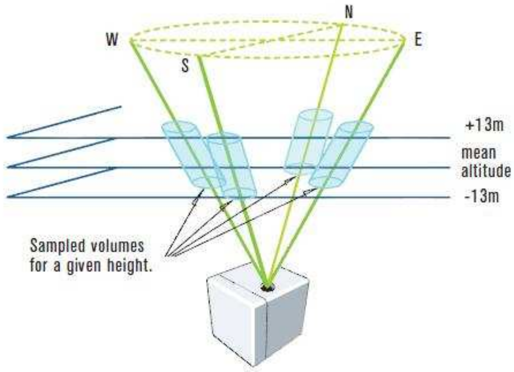

Figure 5.4.1: Sample Volume Doppler LIDAR Retrieval, [15]

Electrical	
Power supply	24V DC or 100/240V AC 50-60 Hz
Power consumption	111W to 375W
Environmental	
Temperature range	-30°c to +40°c (with winter package)
Operating humidity	IP65
Rain protection	Wiper
Compactness	Portable
Optics & Electronics	
Laser	Class 1 - 1,54 µm
Eye safety	IEC 60825-1
Dimensions	
Size	800x550x550 mm
Weight	60 kg
Data	
Data format	ASCII / binary
Data transfer	GSM / GPRS / LAN / TCP-IP

Figure 5.4.2: windcube specifications, [15]

5.5 Selected Anemometer

The chosen anemometer had been mounted on the top of the nacelle of the WTG number four. It is manufactured by the German company "Thies Clima" (number 4.3351.00.000) and classified by IEC 61400-12-1 as a "First Class" anemometer. A picture of this conventional cup anemometer can be seen in figure 5.5.1.

Figure 5.5.1: cup anemometer , [16]

Chapter 6

Test Series

6.1 Use of Windcube

The series of measurement started on the 7th of July 2010. The mounting of the windcube started at around 8 am and was finished at 11:30 am. A 230V grid connection served as a power supply, connected to the wind turbine number 4 and sloping unseen through the adjacent fields. The windcube was located within a cornfield. Thus, the sight from the path along the fields to the windcube was limited. Additionally, the system was equipped with a ground anchor, circled by a fence (see figure 6.1.1) and equipped with a GPS detection system to reduce the risk of burglary.

Figure 6.1.1: windcube measuring wind speeds in Bruck, [12]

The series of measurement started immediately after the installation. Unfortunately the cooling unit of the windcube under use was not working properly. As the temperatures in the following days had been very high and the wind velocities had been rather low, the system shut down automatically due the danger of overheating. It then had to be started manually. Therefore the series of measurement was interrupted several times. Even the mounting of a shield to block the sun (see figure 6.1.1) could not prevent the system from overheat. After the windcube had been exchanged and the new system performed reliable. Figure 6.1.2 shows the considered wind turbine and the windcube.

Figure 6.1.2: Wind turbine and windcube, [12]

The system was focused on nine different measurement heights (see also on figure 6.1.3): 40, 65, 70, 85, 100, 135, 160, 185 and 200m above ground level.

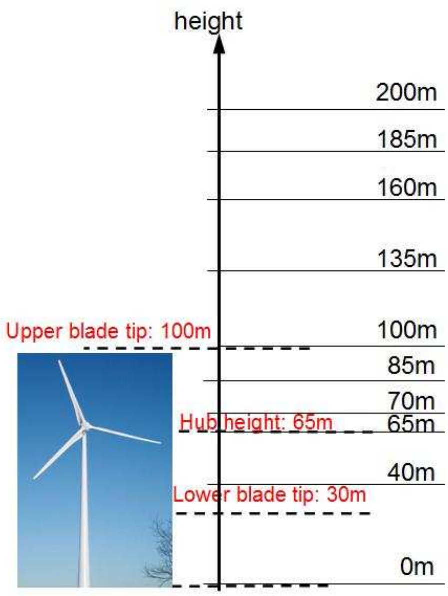

Figure 6.1.3: measurement heights

Figure 6.1.4 shows a windcube data file. A description of its contents can be seen in figure 6.1.5.

```
10mindaten - Editor
Datei  Bearbeiten  Format  Ansicht  ?
HeaderLength=55
Version=2.1.58
ID System=WLS7-70
ID Client=Meteotest
Localisation=0
GPS Localisation=0
Comments=
Measurements informations :
********************
ScanAngle(°)=27.37
NumberOfAveragedShots=10000
RollAngle(°)=0.00
HeadingAngle(°)=0.00
Altitudes(m)=   40      50      60      80      100     120     140     160     180
PitchAngle(°)=0.00
CNRThreshold=-22
WiperCNRThreshold=-19.0
WiperAltitude(m)=100.0
WiperDuration(ms)=1000.0
Wavelenght(nm)=1543.00
Angle BetweenTwoPositions(°)=90
DirectionOffset(°)=0.000
Algorithm Parameters :
********************
Algorithm=MLE
MAOFrequency(Hz)=67900000.000
CutOffFrequency(Hz)=90000000.000
WindowLength(s)=0.000000E+0
IndexRange0=66
PathLaserPulse=C:\Documents and Settings\user\Desktop\TOOLS\DistCalib\AcqirisRun_2009-12-16T16-10-58\pulse_laser.sig
NumberOfSamples_LaserPulse=74
BeginIndex_LaserPulse=0
BeginIndex_NoiseReference=0
NumberOfNoiseWindowsByProfile=1
VrThreshold (m/s)=)1.700
SigmaFreqThreshold (m/s)=)0.750
Acquisition Parameters :
********************
SamplingInterval=4.000000E-9
NumberOfSamples=1024
VerticalCoupling=AC, 50 Ohm
Offset=0.000
FullScale=0.200
NumberOfSegments=100
TriggerSource=External
TriggerCoupling=DC, 50 Ohm (Ext. trig. only)
TriggerSlope=Positive
TriggerLevel1=3000
TriggerLevel2=0
DelayLine=4.000000E-7
AbsoluteInitialPosition(°)=102690
RelativeInitialPosition(°)=90
InitialDate/Time=05/02/2010 01:01:01.35
Gain=32.797000
InitialLD1(mA)=IC1=290
InitialLD2(mA)=IC2=1400
Date    WiperCount      Tm      Vhm1    dvh1    VhMax1  VhMin1  Azim1   um1     du1     vm1     dv1     wm1     dw1     CNRm    dCNR    CNRmax  CNRmin  sigmaFreqm
```

Figure 6.1.4: example of a windcube data file

- Data stored in this file are the following (Fig. 16):

- 1st column: Date is data timestamp
- 2nd column: Tm is the average temperature over the past 10 minutes
- 3rd to 20th columns: data relative to first altitude (40m in example above) including, column by column:
  - Vhm1: 10 minutes averaged horizontal wind speed [m/s]
  - dVhm1: Variance on horizontal wind speed
  - Vhmax1: Maximal horizontal wind speed during the past 10 minutes [m/s]
  - Vhmin1: Minimal horizontal wind speed during the past 10 minutes [m/s]
  - Azim1: 10 minutes averaged wind direction [rd]
  - um1: 10 minutes averaged wind vector projection along x-axis [m/s]
  - dum1: Variance for previous value
  - vm1: 10 minutes averaged wind vector projection along y-axis [m/s]
  - dvm1: Variance for previous value
  - wm1: 10 minutes averaged wind vector projection along z-axis [m/s]
  - dwm1: Variance for previous value
  - CNRm1: 10 minutes averaged CNR (Carrier to Noise Ratio) [dB]
  - dCNRm1: Variance for previous value
  - CNRmax1: Maxima horizontal CNR during the past 10 minutes [dB]
  - CNRmin1: Minimal horizontal CNR during the past 10 minutes [dB]
  - sigmafreq1:10 minutes averaged spectral broadening [converted to m/s]
  - dsigmafreq1: Variance for previous value
  - Avail1: Raw data availability during the last 10 minutes
- 22th to 39th columns: data relative to second measurement above classified as in columns 3 to 20
- ...

Figure 6.1.5: description of the parameters within a windcube data file

6.2 Enercon Scada

Enercon Scada is a remote monitoring system offering WTG data. Parameters like power output and wind speed (which is gained by mathematical analysis of rotor torque and the hub mounted Enercon anemometer) can be obtained. Figure 6.2.1 shows an example of ten minute averages provided by Enercon Scada. The first column represents the date, the second the average wind speed, the third the maximum wind speed and the fourth the minimum wind speed. Column number five (E) contains the average power.

	A	B	C	D	E
1	Datum	mittl, Windgeschw, [m/s]	max, Windgeschw, [m/s]	min, Windgeschw, [m/s]	mittl, Leistung [kW]
2	01,07,2010 00:00:	3,16	4,3	1,8	22,4
3	01,07,2010 00:10:	3,56	5,2	2,3	31,2
4	01,07,2010 00:20:	3,88	5,2	2,6	41,4
5	01,07,2010 00:30:	4,33	5,9	3,2	62,7
6	01,07,2010 00:40:	4,89	6,6	3,1	105,2
7	01,07,2010 00:50:	4,79	6,5	3,6	92,8
8	01,07,2010 01:00:	4,73	6,5	2,8	81,6

Figure 6.2.1: example of an Enercon Scada data file

6.3 Additional Data

As discussed in chapter 7 information about the temperature and air pressure is necessary in order to calculate the power curves. The Austrian Central Institute for Meteorology and Geodynamics called "ZAMG" provided these data. The weather station was located in Bruck Neudorf and therefore in close proximity to the wind park.

Chapter 7

Analysis

7.1 Preparation

The analysis of the data needed some preparation. First, the data was gathered, second, the different data files needed to be put together in one single file and third, the time series needed to be synchronized. This part of the work proved to be very time consuming and needed a lot of care. Many data sets were not complete. Often some lines were missing, sometimes additional lines with different time scales appeared. Therefore the Microsoft software "MS Excel" was used, which provides easy handling and a good overview of comprehensive data sets. Additionally some of the algorithms had been implemented in MS Excel, see chapter 7.2. Other calculations were performed in the numerical computing environment called "Matlab".

7.2 Calculation

According to the ideal gas law temperature and pressure determine the number of particles within a certain volume. The number of certain particles within a volume then determines the density of a certain gas. This density influences as seen in equation 2.1.4 the energy within an airflow and therefore also the power to be gained by a WTG. Each warranted power curve thus underlies a certain air density. This density is normally defined as: $\rho = 1.225 kg/m^3$. Deviations from this density need to be corrected by adjusting the data to standard conditions. This process is called normalization and is shown in chapter 7.2.1.

7.2.1 Normalization of Data

If air temperature and pressure are known, the actual air density can be calculated by the following equation[1]:

$$\rho_H = \rho_0 \cdot \frac{288.15}{273.15 + t} \cdot \frac{p_H}{p_0} \tag{7.2.1}$$

In order to calculate a power curve according to standard conditions the wind speed needs to be corrected as seen in equation 7.2.2.

$$v_{norm} = v \cdot \left(\frac{\rho_H}{\rho_0}\right)^{1/3} \tag{7.2.2}$$

The normalization was done for the complete series of measurements. The magnitude of this correction depends upon the environmental circumstances during the series of measurements.

7.2.2 Determination of Power Curves

IEC 61400-12-1 provides a statement of requirements for the measurement of power curves using cup anemometers. As LIDAR systems are based upon volume measurement and their results are vectors instead of scalars, those requirements cannot be met by LIDAR systems. IEC is currently working on a standard for remote sensing instruments to fill this gap. Still, wherever possible, the standards set within IEC 61400-12-1 were fulfilled during the measurement. For instance the distance of the measuring system and the interested monitored WTG needs to be between two and four rotor diameters, which was carefully considered in this series of measurement. After the normalization of the data, a high number of data points was gained. The next step was to find a best fitting curve. Often a least square fit is used to set the parameter of a given mathematical function. In case of power curves no mathematical function describing the curve exists. Actually this function shall be determined. IEC 61400-12-1 mentions the method of bins to solve this problem, which will be discussed within the next paragraphs.

Interpolation

The Matlab function "splines" was performed. This allowed a least square fit of polynomial functions. After sampling the function parameters the results were promising. More details can be seen in the Matlab code, which is located in the appendix.

[1]this standard is set by IEC 61400-12-1; influence of the moisture of air is not taken into consideration

Method of Bins

Stated briefly, for the method of bins the data is scaled into wind speed intervals and arithmetically averaged within those intervals. The outcome of this method is a very low number of data points which shall correlate strongly with the raw data. The interval deviation provides information about the reliability of the data.

During the calculation both methods (Interpolation and method of bins) had been applied to the data. As there is currently no standard for remote sensing, both methods were performed and compared. The calculation of the method of bins was facilitated by a Visual Basic for Applications script within Excel. The code can be seen inside the appendix.

7.2.3 Energy Yields

After the power curves had been calculated the next step was to determine the influence of differences between power curves on the energy yield. Therefore a certain wind distribution needed to be assumed. The Weibull distribution gives a fitting probability density function for wind distributions, see equation 7.2.3.

$$wdf(v) = \frac{k_{wdf}}{A_{wdf}} \left(\frac{v}{A_{wdf}}\right)^{k_{wdf}-1} exp\left(-\left(\frac{v}{A_{wdf}}\right)^{k}_{wdf}\right) \tag{7.2.3}$$

Within Austria, the parameter k_{wdf} equals the number 2 unless stated otherwise. Assuming $k_{wdf} = 2$ the parameter A_{wdf} was determined by the average wind speed. If the power curve is multiplied with the wind speed probability density function the result is an energy density function. As each computational program only supplies discrete calculating intervals, the distributions needed to consist of discrete values. The wind speed was set from $0m/s$ to $25m/s$ with steps of $0.01m/s$. The energy yield was calculated by the summation of those 251 elements within the wind energy distribution divided by the sum of the 251 elements of the wind speed probability density function. Multiplying by a time component (24hours multiplied with 365 days=$24 \cdot 365h$) and an availability ($\eta_{av} = 97\%$) resulted in an yearly energy yield. The Matlab code can be seen inside the appendix.

7.2.4 Wind Shear

The calculation of wind shear was implemented in Excel. The scalars of the horizontal wind speeds had been summarized for each height. Dividing by number of data points resulted in an arithmetic mean for each measurement height. It happened rather often that data in heights of about 200m were not available as a result of a bad CNR. These results were then filtered by a Visual Basic for Applications script. The code can be seen inside the appendix.

7.3 Accuracy

As the measurement campaign included comprehensive data several error sources shall be mentioned, which could have had a significant influence on the results. An exact quantification of the influence of each error source should have taken comparative measurements for longer time period and a very sophisticated mathematical treatment. However, this is beyond the score of this thesis. Still, possible error sources shall be mentioned.

The LIDAR system windcube has, as every measuring system, a limited accuracy. The measurement of the wind speed is expected to be very accurate under optimal conditions. The error should be less than 0.2 m/s at each measurement height. Still turbulent, bad weather conditions and low CNR could have decreased the accuracy of the system.

Data gained by the Enercon Scada system is also subject to inaccuracies. The data points within figure 8.1.1 do not reproduce the power curve exactly, which may be interpreted as measurement inaccuracies and/or fluctuating wind conditions. Interpolation of this data sets shall reduce the influence of these inaccuracies.

The data set received by the austrian "Zentralanstalt für Meteorologie and Geodynamik" (ZAMG), containing values for air pressure and temperature, can be considered as sufficiently accurate. First, the systems in use by ZAMG have a very high accuracy, second, the influence of small deviations are very low because the mathematical algorithm applied upon this data was minimizing its influence.

The local arrangement of the measuring systems also has an influence. The deceleration of the wind as it approaches the wind turbine already contributes to energy production. Therefore the measurement system must be placed in a predetermined distance from the turbine. Under certain conditions the wind speed measured at a distance from the turbine may not be the same as the speeds experienced at the turbine. Wakening effects and influences due to the orography can affect the measurement significantly.

The mathematic algorithms used are based upon physical models. Each model is an abstraction of reality with built in assumptions and simplifications. In order to calculate the power curves the data sets had been filtered. Wind speeds had been normalized, quantified and processed. Wind distributions were assumed and used to calculate energy yields. Each step includes simplifications which may contribute an amount of error. Still, this does not effectively means that the results of this measurement have reduced expressiveness. Actually, higher deviations of the data points present in figure 8.1.2 can be better understood. Figure 8.1.1 is based upon Enercon Scada data, ZAMG data and mathematical algorithms whereas figure 8.1.2 includes additional data derived from the LIDAR system, which also represents an error source.

In short, the following factors influence the accuracy of the results of the measurements:

- inaccuracies of the LIDAR system - turbulence, weather conditions, low CNR
- inaccuracies of the Enercon Scada system
- local arrangement of the LIDAR system - wakening effects and orography
- simplifications and assumptions included in physical models and mathematic algorithms

Chapter 8

Evaluation

This chapter contains

- the results of the analysis of the series of measurement and
- an explanation and discussion of these results

The measured power curves, wind shear, calculated energy distribution and yields are presented here. Furthermore two different wind distributions are considered (case 1 and 2) to examine the relationships between the power curve, wind distribution and energy yield. Additionally, suggestions that may improve the wind park design are elaborated.

8.1 Measured Power Curves

As already mentioned two different data sources were available for the determination of the power curve. First, the Enercon Scada data was available since the WTG were owned by VERBUND Renewable Power GmbH. Second, the LIDAR data was available from the 07th of July up to the 6th of October including some interruptions. With this data, different power curves were calculated (Scada and LIDAR, normalized and not normalized) and compared with the warranted[1] power curve.

[1] The warranty of the power curve has already expired. Therefore the analysis is just of theoretical interest and not connected with any consequences concerning the manufacturer

8.1.1 Power Curve: Scada

Figure 8.1.1 shows the power curve for the Enercon Scada data set.

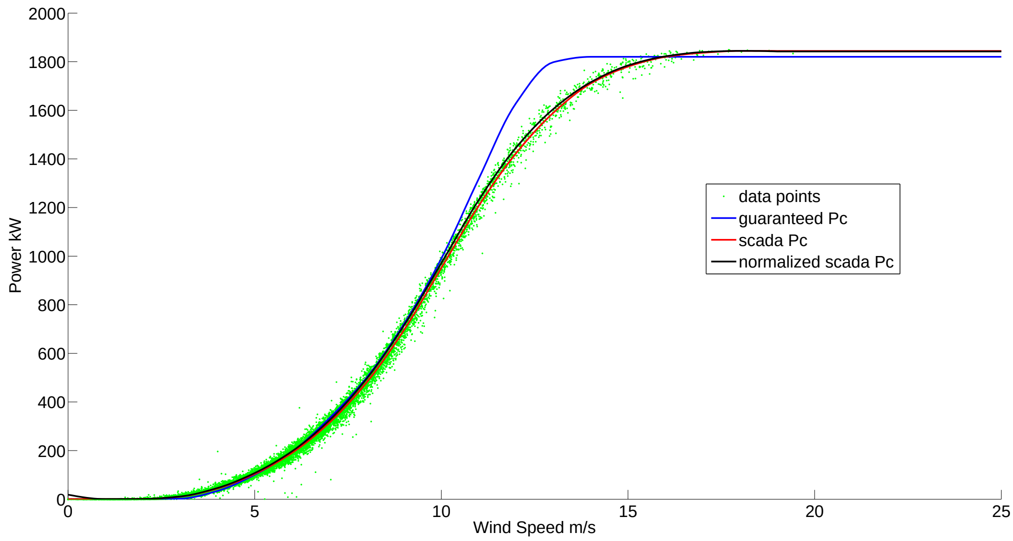

Figure 8.1.1: Power curve for Enercon Scada data set

The data points can be seen in green, the warranted power curve in blue, the Scada power curve in red and the normalized Scada power curve in black. The data points show the non-normalized data set which fits very well with the red line, indicating only minor deviations. Normalization of the data, black curve, indicates no vigorous change. Between 10 and 15m/s a small gap can be seen. Due to the hot summer days with increased temperature during the measurement the air had been less dense and therefore normalization shifted the power curve gained upward. Still the warranted power curve is not fulfilled. For wind speeds between 10 and 15m/s strong differences are evident. Interestingly the maximum power of the Scada power curve is higher than the maximum power of the warranted curve.

8.1.2 Power Curve: LIDAR

Figure 8.1.2 shows the power curve based upon the LIDAR data set.

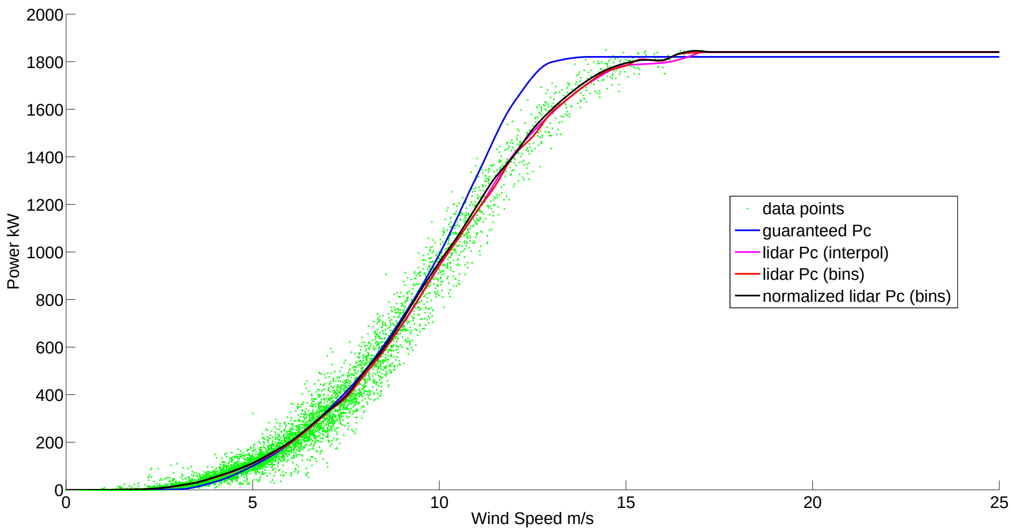

Figure 8.1.2: Power curve based upon LIDAR data set

The data points can be seen in green, the warranted power curve in blue, the interpolated LIDAR power curve in pink, the LIDAR power curve based upon the method of bins in red and the normalized LIDAR power curve based upon the method of bins in black. If the data points are compared with the data points in figure 8.1.1 a lower number of data points and high deviation is evident. Still the calculated power curves look rather similar to the Scada power curve. Whether the power curve is calculated by the method of bins or by interpolation, the result is almost the same. The calculation based upon the method of bins shows a weak ripple which can be explained by the low number of data points. The normalization of the power curve has little influence.

8.1.3 Comparison of Power Curves

Figure 8.1.3 shows the warranted power curve in blue, the normalized Scada power curve in red and the normalized LIDAR power curve in black.

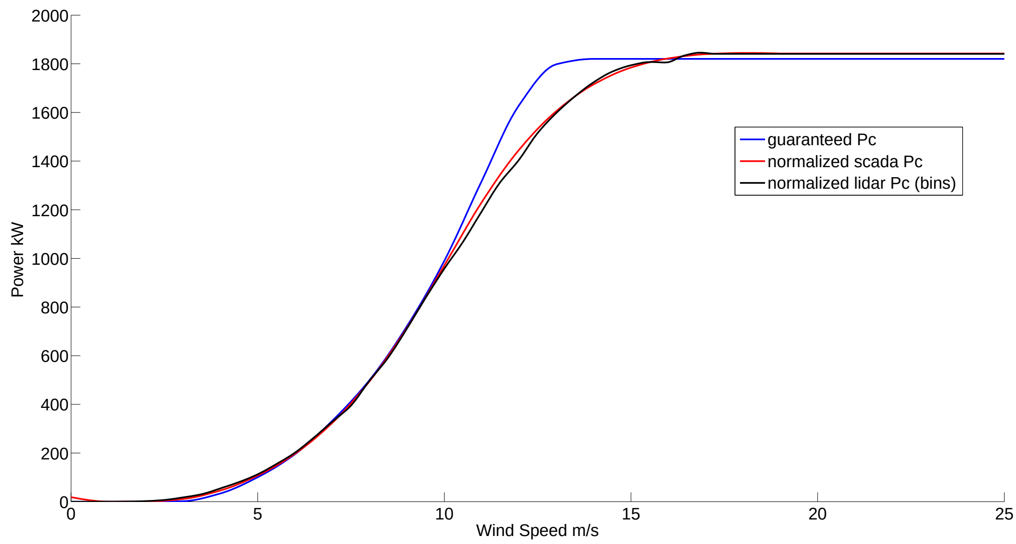

Figure 8.1.3: Comparison of power curves

It can be seen that the LIDAR power curve fits much better to the Scada power curve than to the warranted one. Moreover, the LIDAR power curve is even worse. There is strong evidence, that the real power curve does not agree with the warranted power curve. A measurement meeting the standards of IEC 61400-12-1 may deliver equivalent results. Most manufactures are liable for the loss of payments (if reasoned by a insufficient power curve). If the warranty were still valid, the loss needs to be calculated. Normally this is done retrospectively.

8.2 Measured Wind Shear

The measured wind shear can be seen in figure 8.2.1. It spreads from $5.5m/s$ at a height of $40m$ up to $8m/s$ to a height of $200m$. As the blade tips reach from $35m$ up to $100m$ of height the rotor swept area is also exposed to the wind shear. Facing this, the conventional measuring method of mounting a cup anemometer in hub height in a given distance seems improper with ever larger turbines which incorporate stronger influences of wind shear and increasing rotor swept areas. Knowledge of the wind shear may also be used to optimize the wind park design. First, the hub heights can be chosen more carefully, and second, the selection of appropriate rotor diameters and rated powers of the WTGs can be tailored to improve performance.

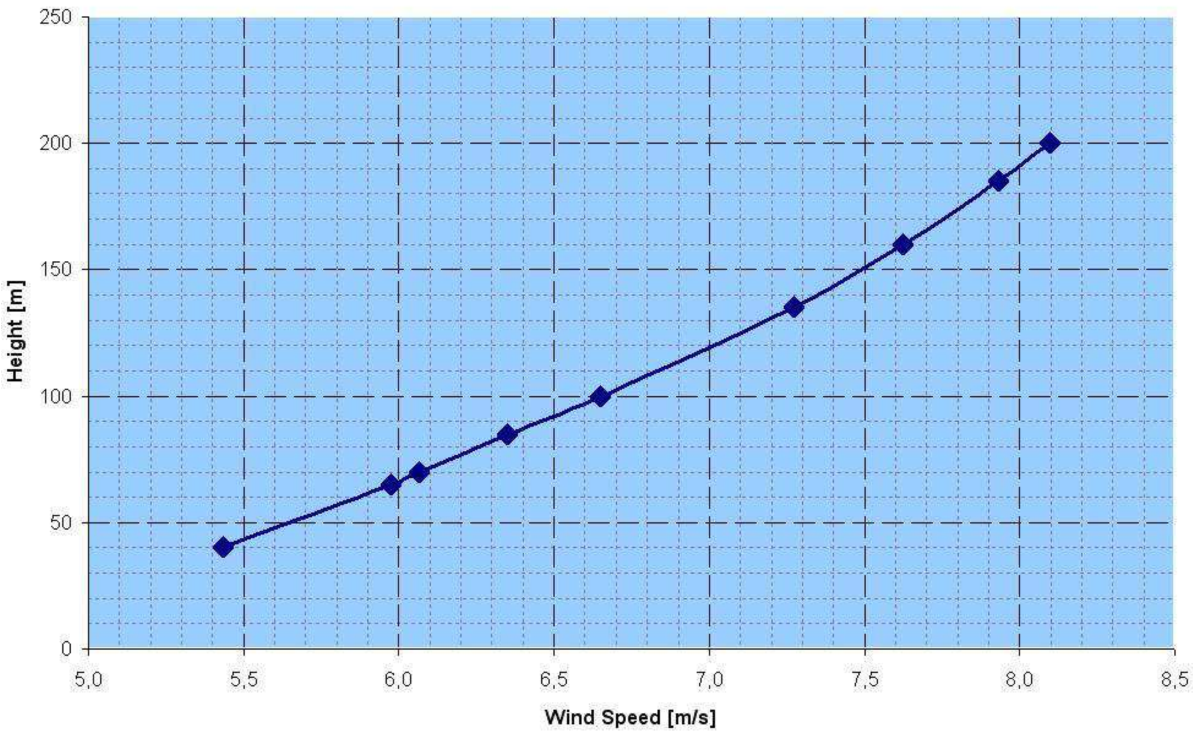

Figure 8.2.1: Measured wind shear

8.3 Calculated Wind Distributions

The knowledge of wind distributions allows the calculation of energy densities and energy yields for a given time period. If the wind distribution function is chosen carefully, the information gained by yield calculation is of great value for wind park design. Figure

8.2.1 shows the wind shear on the Bruck project site. As the average wind speed[2] in hub height was about $6m/s$ and the average full load hours of the WTG was approximately $1850h/a$ the curve parameter A_{wdf} of the Weibull probability density function has been set to 7.11. The calculated full load hours based upon the LIDAR power curve are in this case (realistic case 1) $1887h/a$ and the average wind speed is $6.3m/s$. As the wind shear has strong influence on the average wind speed, a second case (fictive case 2) was calculated, assuming a hub height of 200m and an average wind speed of $8m/s$. Therefore the parameter A_{wdf} was set to $A_{wdf} = 9.03$. The probability density functions of both cases are shown within the following subchapters.

8.3.1 Case 1

Figure 8.3.1 shows the Weibull probability density function with the parameter set: $k_{wdf} = 2$ and $A_{wdf} = 7.11$. This case is very close to realistic circumstances, and therefore was used as a reference for the calculation of actual energy yield losses.

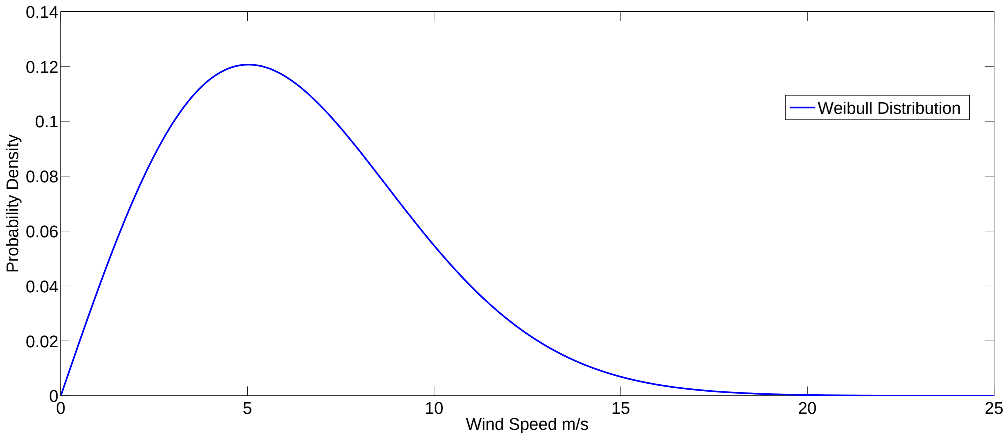

Figure 8.3.1: Weibull probability density function case 1

8.3.2 Case 2

Figure 8.3.2 shows the Weibull probability density function with the parameter set: $k_{wdf} = 2$ and $A_{wdf} = 9.03$. As mentioned a fictive case is represented by those parameters, assuming a hub height of $200m$.

[2]during the series of measurements

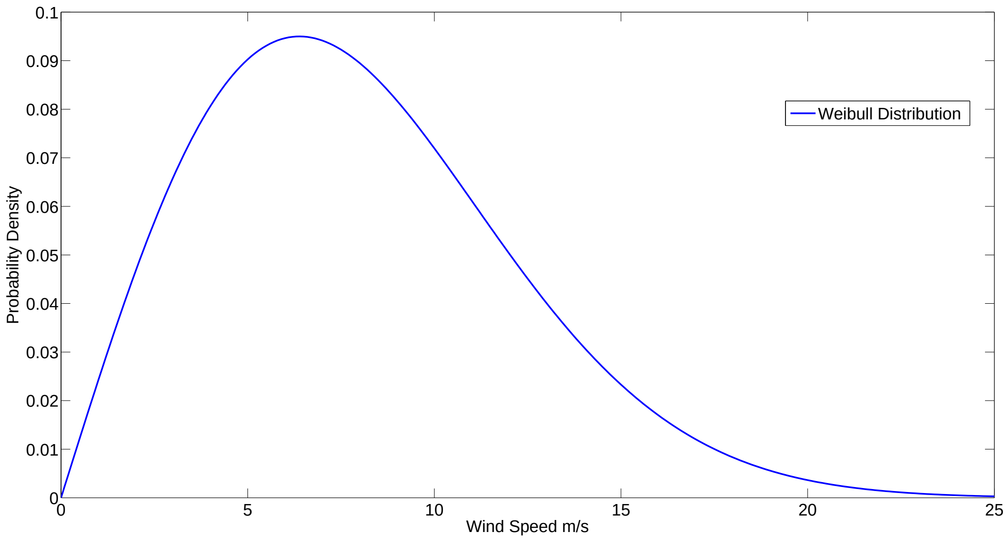

Figure 8.3.2: Weibull probability density function case 1

8.4 Calculated Energy Distributions

If the power curve is multiplied with the wind distribution the result is an energy distribution. The next subchapters show different energy distributions for both cases.

8.4.1 Case 1

Figure 8.4.1 shows the energy distributions of the calculation based upon the warranted power curve (blue), the normalized Scada power curve (red) and the normalized LIDAR power curve (black) and the wind distribution from figure 8.3.1. Although the calculated power curves differ strongly from the warranted for a wind speed of $13m/s$, the energy distribution is almost similar for this speed. This can be explained due to a weighting affect as a result of the multiplication with the wind distribution. Wind speeds of around $13m/s$ are not as frequent as lower wind speeds, as can be seen in figure 8.3.1. The areas underlying the energy density functions are equivalent to the energy yield within a given period of time. Based upon the shape of the curves it already can be estimated, that they differ by only a few percent.

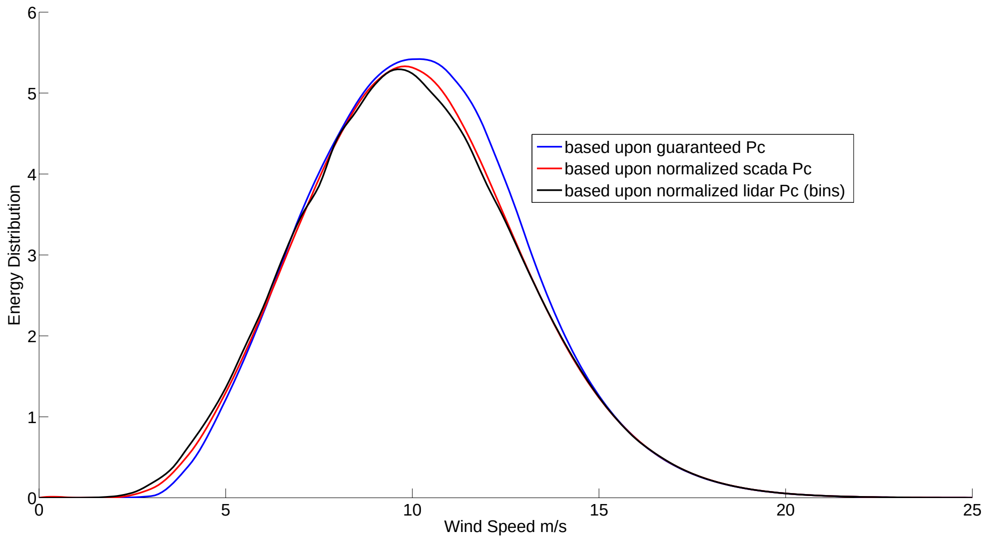

Figure 8.4.1: Calculated energy distribution case 1

8.4.2 Case 2

Figure 8.4.2 shows the energy distributions of the calculation based upon the warranted power curve (blue), the normalized Scada power curve (red) and the normalized LIDAR power curve (black) and the wind distribution 8.3.2. Compared to case 1 the functions are shifted to higher wind speeds and have a higher peak amplitude and a wider distribution. The gap between the "warranted" and the calculated energy densities has increased for wind speeds of approximately $12.5m/s$. This shows that the influence of different power curves cannot be predicted exactly without the knowledge of a certain wind distribution.

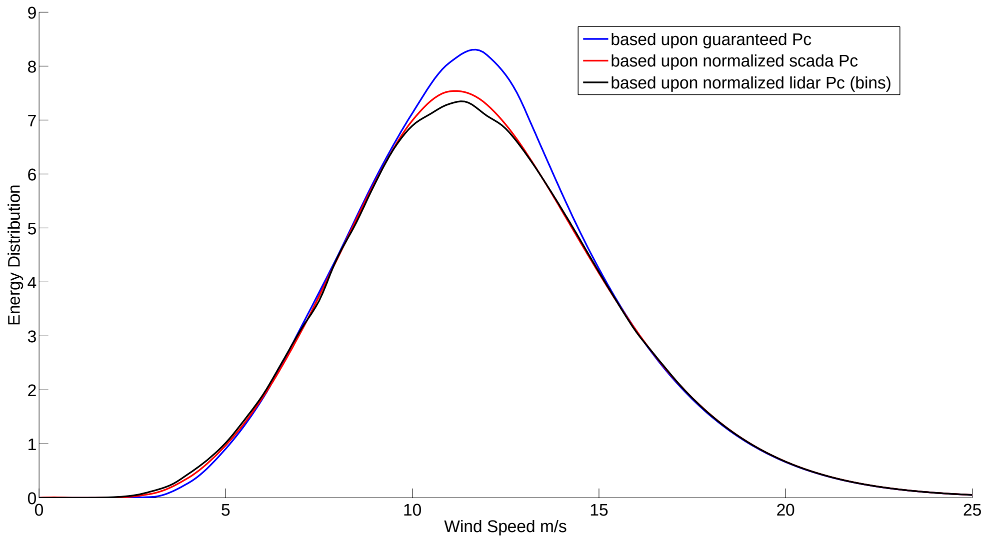

Figure 8.4.2: Calculated energy distribution case 2

8.5 Calculated Energy Yields

The areas underlying the energy density functions are equivalent to the energy yields within a certain period of time. This period was set to one year for the following calculations.

8.5.1 Case 1

Figure 8.5.1 shows different energy yields in case 1. The calculation based upon the warranted power curve was used as a reference and represented 100% of energy yield. Despite rather strong differences in power curves, the difference in energy yield are below 6 percent. The effect of normalization could also be seen. A further detailed analysis follows in chapter 8.6.

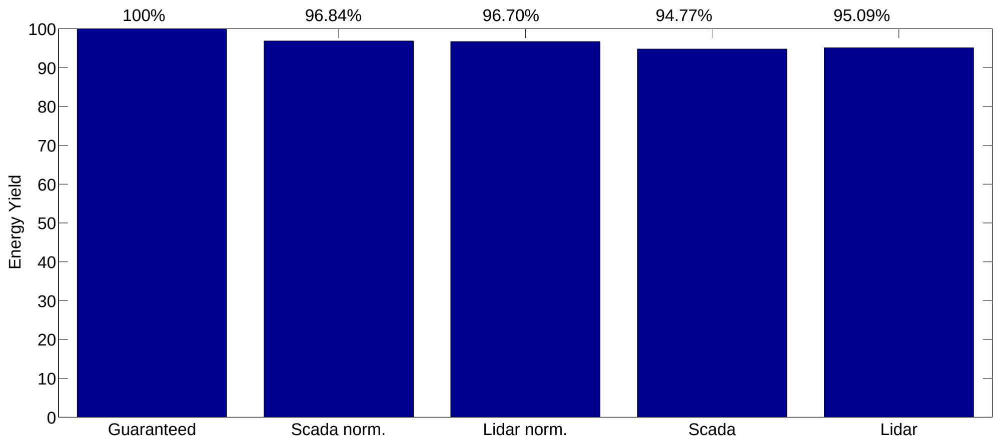

Figure 8.5.1: Calculated energy yields case 1

8.5.2 Case 2

Figure 8.5.1 shows different energy yields in case 2. As already recognized during the discussion of the energy densities the energy losses are higher than in case 1 (absolute as well as relative).

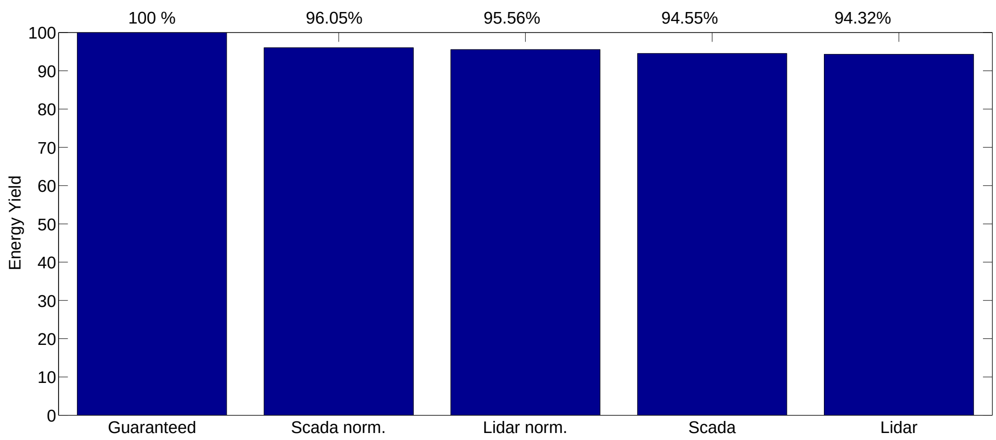

Figure 8.5.2: Calculated energy yields case 2

8.6 Final comparison of Case 1 and Case 2

The table shown in figure 8.6.1 contains the results of the calculations. Considering case 1, the annual energy yields are about 3.3 Mio kWh which equals about 1900 full load hours. The comparison of the results based upon three different power curves (warranted, Scada, LIDAR) shows the influence on the energy yield. If the yield gained by the warranted power curve represents 100 percent, the Scada power curve leads to a yield of 96.74 percent. The LIDAR power curve results in a yield of 96.16 percent, which is even less. A loss of 3.26 or 3.84 % in yield and revenues is remarkable.

The second case shows a similar scenario. The losses are even higher (4.02 and 4.81 %). Although the wind energy flowing through the WTG has increased in this case by 203 % the yields rose by only about 64 %. The WTG is not able to completely harvest the additional winds due to the limits of the rated power. The high number of full load hours can be considered as a hint that larger wind turbines with higher rated power may increase the energy yield and the performance of the fictive wind park. This scenario could be calculated by adding new power curves. The last column in both tables represents the average power of the WTG, which is proportional to its full load hours. In modern wind park design, main wind directions, orography and the influence of wake effects also need to be considered.

	Case 1			Case 2		
	Guranteed	Scada norm.	LIDAR norm.	Guranteed	Scada norm.	LIDAR norm.
Energy Yield (Mio. kWh/a)	3,43	3,32	3,31	5,65	5,43	5,40
Percentage	100	96,84	96,70	100	96,05	95,56
Percentage vs case 1	-	-	-	165	164	163
Full Load Hours (h/a)	1963	1901	1899	3237	3109	3093
Average Power (kW)	403	391	390	665	639	636

Figure 8.6.1: Final results case 1 and case 2

Chapter 9

Comparison with other Methods of Power Curve Measurement

The process of certified measurement of power curves is described within IEC 61400-12-1. First class cup anemometers mounted at hub height at a given distance are used to measure the horizontal wind speed. The data needs to be normalized and the power curve needs to be calculated by the method of bins. Additionally, deviations within each bin shall be calculated.

As LIDAR measurements are volume based rather than punctual measurements, information gained by LIDAR systems are different. Wind shear within the rotor swept area (see figure 9) can be measured. This allows the calculation of an equivalent average horizontal wind speed, which represents realistic wind conditions better than a single anemometer. With ever larger turbines, the influence of wind shear increases. Since the pitching system of a WTG can only adapt to unique wind speeds, wind shear always leads to suboptimal force distributions on the rotor blades and thus decreased power coefficients. Still, conventional measurement approaches focusing horizontal wind speeds on hub heights may have produced favorable power curves from a manufacturer point of view. As wind power increases cubically with wind speed, higher speeds on the upper area of the turbine have more influence than lower speeds downwards. These considerations are actually discussed by the IEC. New standards for adequate power curve measurements using remote sensing technologies might be set within the next years.

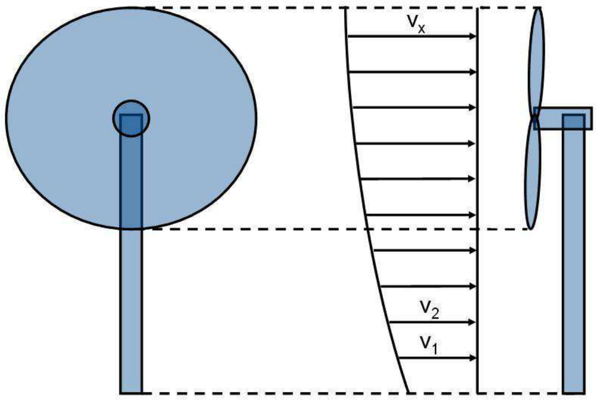

Figure 9: Rotor swept area and wind shear

Aware of the assumptions taken in the calculations in this thesis it shall be pointed out that those thoughts had not been implemented. The power curve calculation was based upon the measured horizontal wind speed at hub height and handled as if it were punctual. Otherwise calculations would have blasted the context of this master thesis. New approaches are still object of discussion.

Despite all the taken simplifications during this work the results are still promising. Remote sensing technology seems to bear great potential for wind speed determination applications.

Chapter 10

Outlook and Discussion

This LIDAR campaign based upon Doppler Wind LIDAR was the first of its kind in Austria. Although some appliances seem to have teething troubles the potential of the technology is great. Doppler Wind LIDAR systems deliver reliable data wherever homogenous wind conditions are dominant. Further, development may also increase the performance of the system in complex terrain.

The verification of power curves based upon remote sensing technologies is not finally developed yet. Approaches close to anemometer technology are possible and lead to satisfying results, but face ever larger rotor diameters additional information gained by remote sensing shall be implemented.

Compared to met masts LIDAR systems are easily installed and have strong advantages in terms of price and bureaucratic effort in case of short time campaigns. No building permission is necessary for mounting a LIDAR system. On the other hand maintenance might be necessary. This may include refilling the tank of a diesel generator in case of green field projects or the refilling of the wiper tank. One great advantage of LIDAR systems is their compact size which allows easy transportation and installation. Due this compactness the system is unfortunately also at risk of burglary. Therefore the system needs to be secured on the project site. Depending on the location of the project site considerable effort needs to be taken for its securement. Enercon has developed a men-sized box which holds the LIDAR system and further equipment. This strongly increases the security, but also leads to a higher logistic effort due the sheer size of the complete system. Long time measurement campaigns are rather expensive for the rental costs are very high. Further commercialization may decrease these costs. Extensive site assessment may include long time measurement data from met masts which is complemented by short time measurement data provided by ground based LIDAR systems. A complete abandonment of met masts for site assessment is nowadays not conceivable, but this might change with further commercialization of the systems.

Additional applications of LIDARs may appear with increased commercialization. Research is done on the field of hub mounted systems, allowing the prediction of wind speeds for several seconds in advance. This makes pre-pitching possible, in which the information gained about the wind profile is used to choose a fitting pitch. An increase of yield as well as reduced mechanical forces are the result of this technology. Eventually Doppler wind LIDARs may also find use in other industries like aircraft or meteorology.

Chapter 11

Conclusions

The emission and detection of electromagnetic waves bears several advantages over Doppler wind LIDAR as a remote sensing technology. The accuracy is sufficing for most wind conditions although the technology is rather young and not yet commercialized. Even within the market of Doppler LIDAR systems competing technologies exist (pulsed and continuous waves). Therefore further development and technical advances can be expected to increase the accuracy and reduce the power consumption, which is of interest in case of green field projects.

The Doppler wind LIDAR "windcube" offered reliable data allowing the determination of the power curve according to IEC 61400-12-1. In comparison to cup anemometers, which are measuring a scalar representing the wind speed at a specific point, LIDAR systems are measuring the velocity vector within a certain volume. Therefore comprises needed to be taken to follow IEC 61400-12-1. A new standard for remote sensing technology can be expected in the future. Still, the results of the power curve determination corresponded with the calculation based upon the Scada monitoring system.

As different data sources were implemented in the calculations the experimentalist needs to take special care to secure time synchronization. Several data sets with missing lines or different time scales appeared, which had to be excluded manually. The calculation itself was straight forward.

Summarizing the first Doppler wind LIDAR campaign in Austria, following pros and cons can be mentioned beginning with the pros:

- easy transportation and installation
- reliable data
- different measurement heights up to 200m

- allowing analysis of the wind shear

Cons:

- high price for long time measurement
- no standards exist to date
- risk of burglary

The pros of LIDAR technology are outweighing the disadvantages. Easy transportation and installation gives an excellent opportunity for short time measurements. The measurement of different heights provides more detailed information and allows the analysis of the wind shear. Commercialization of the systems may reduce its prices reducing also the risk and harm of burglary. Standards will be set by IEC, who is working nowadays on standards providing clear instructions for the analysis of data gained by remote sensing technology. Results can be expected within the next years.

Concluding these thoughts the LIDAR campaign run by VERBUND in cooperation with Meteotest can be considered as a success opening possibilities for further experiences within the company.

Bibliography

[1] **Author: E. Hau** *Wind Turbines - Fundamentals, Technologies, Application, Economics*, Springer, 2006.

[2] **Author: T. Ackermann** *Presentation on Wind Turbines*, Energynautics, 2008.

[3] **Author: E. Hau** *Wind Turbines - Fundamentals, Technologies, Application, Economics*, Springer, 2000.

[4] **Author: E. Hau** *Windkraftanlagen: Grundlagen, Technik, Einsatz, Wirtschaftlichkeit*, Springer, 2008.

[5] **Author: Georg A. Reider** *Photonik - Eine Einführung in die Grundlagen*, Springer, 2004.

[6] **Author: G. Fasching** *Werkstoffe für die Elektrotechnik - Mikrophysik, Struktur, Eigenschaften*, Springer, 2005.

[7] **Author: G. Strasser** *Halbleiterphysik*, Lesson Script, 2006.

[8] **Author: K. Seeger** *Semiconductor Physics: an introduction*, Springer, 2004.

[9] **Author: C. Weitkamp** *Lidar: range-resolved optical remote sensing of the atmosphere*, Springer, 2005.

[10] **Author: C. Hofstetter** *Graphic created by the author, C. Hofstetter*, 2010.

[11] **Author: T. Mikkelsen et al** *12MW: final report*, Paper, 2009.

[12] **Author: VERBUND AG** *Graphic provided by VERBUND AG*, 2010.

[13] **Author: ENERCON GmbH** *Data provided by ENERCON data sheet*, 2000.

[14] **Author: NATURAL POWER** *Graphic and data provied by NATURAL POWER*, 2008.

[15] **Author: LEOSPHERE** *Graphic and data provied by LEOSPHERE*, 2009.

[16] **Author: Adolf Thies GmbH** *Graphic and data provied by Adolf Thies GmbH*, 2009.

[17] **Author: Deutsche WindGuard GmbH** *Evaluation of Windcube*, Paper, 2008.

[18] **Author: M. Wächter et al** *Power curve estimation using LIDAR measurements*, University of Stuttgart- Paper, 2008.

[19] **Author: R. Wagner et al** *Multi-MW wind turbine poewr curve measurements using remote sensing instruments*, Riso Report, 2009.

[20] **Author: K. Träumner et al** *Probing the atmospheric boundary layer with Doppler lidar*, KIT PhD Symposium, 2009.

[21] **Author: T. Mikkelsen** *On mean wind and turbulence profile measurements from ground-based wind lidars: limitations in time and space resolution with continuous wave and pulsed lidar systems*, Review, 2009.

[22] **Author: R. Wagner et al** *Commercial lidar profilers for wind energy. A compartive guide*, Paper, 2009.

[23] **Author: Deutsche WindGuard GmbH** *Comparison of Lidars, German test station for remote wind sensing devices*, Paper, 2008.

[24] **Author: A. Peña** *Sensing the wind profile*, Riso-PhD-Report, 2009.

Appendix
Codes

Matlab Codes

```
%Auswertung der Windmessung

function christian
clear all
close all
clc

%Garantierte Leistungskurve
a=textread('lk_garantiert.txt');
xrange=0:0.1:25;
interpol_gar=interp1(a(:,1),a(:,2),xrange, 'pchip');
%probiere noch lk_g mit spline darzustellen - vielleicht auch besser!

hold on

% Scada gesamtdaten
s=textread('test3.txt');
v=s(:,1);
p=s(:,2);
s_n=textread('test4.txt'); %normierte Daten
v_n=s_n(:,1);
p_n=s_n(:,2);

%Lidar Daten
lid=textread('lk_lidar.txt');
lid_v=lid(:,1);
lid_p=lid(:,2);

% Vektor mit Stützstellen
c=0:0.4:19;
d=0:0.1:19;
r=0:1:19;
c_l=0:0.4:17.5;
```

```
% Parameteranpassung
%scada
phi = spline(c,eye(length(c)),v);
par = phi'\p;

phi_n = spline(c,eye(length(c)),v_n);
par_n = phi_n'\p_n;

%lidar
phi_l = spline(c_l,eye(length(c_l)),lid_v);
par_l = phi_l'\lid_p;

% Approximation
%scada
k = spline(c,par,c)';
l=k;
n=length(k);
for i=4:(n-4)
    l(i,1)=(k(i-3,1)+k(i-2,1)+k(i-1,1)+k(i,1)+k(i+1,1)+k(i+2,1)+k(i+3,1))/7;
end
neu=interp1(c,k,r, 'pchip');
nneu=interp1(r,neu,d, 'pchip');
scada=zeros(1,251);

for i=1:(length(d))
    scada(1,i)=nneu(1,i);
end

for i=(length(d)+1):length(scada)
    scada(1,i)=scada(1,i-1);
end
%scada Normiert
k_n = spline(c,par_n,c)';
neu_n=interp1(c,k_n,r, 'pchip');
nneu_n=interp1(r,neu_n,d, 'pchip');
scada_n=zeros(1,251);

for i=1:(length(d))
    scada_n(1,i)=nneu_n(1,i);
end

for i=(length(d)+1):length(scada_n)
    scada_n(1,i)=scada_n(1,i-1);
end
%lidar
k_l = spline(c_l,par_l,c_l)';
neu_l=interp1(c_l,k_l,0:1:17, 'pchip');
nneu_l=interp1(0:1:17,neu_l,0:0.1:17, 'pchip');
lidar=zeros(1,251);
```

```
for i=1:(length(0:0.1:17))
    lidar(1,i)=nneu_l(1,i);
end

for i=(length(0:0.1:17)+1):length(lidar)
    lidar(1,i)=lidar(1,i-1);
end
hold on
plot(lid_v, lid_p, 'g.')
%plot(c_l,k_l,'k')
plot(xrange, interpol_gar, 'LineWidth',2)
plot(xrange,lidar, 'm', 'LineWidth',2)
%Method of bins Lidar
lidar_bin=textread('lk_lidar_bins.txt');
interpol_lidar_bin=interp1(lidar_bin(:,1),lidar_bin(:,2),xrange, 'pchip');
plot(xrange, interpol_lidar_bin, 'r', 'LineWidth',2)
%plot(lidar_bin(:,1), lidar_bin(:,2), 'rx')
%Method of bins Lidar normiert
lidar_bin_n=textread('lk_lidar_bins_n.txt');
interpol_lidar_bin_n=interp1(lidar_bin_n(:,1),lidar_bin_n(:,2),xrange, '
    pchip');
plot(xrange, interpol_lidar_bin_n, 'k', 'LineWidth',2)
%plot(lidar_bin_n(:,1), lidar_bin_n(:,2), 'kx')
legend('data points', 'guaranteed Pc','lidar Pc (interpol)', 'lidar Pc (
    bins)', 'normalized lidar Pc (bins)','Location','best')
xlabel('Wind Speed m/s')
ylabel('Power kW')

%Einlesen Scada Daten ohne Filter
ss=textread('test2.txt');


figure
hold on
AXIS([0 25 0 2000])
%plot(ss(:,1), ss(:,2), 'b.') %Scada Daten ohne Filter
plot(v,p,'g.') %Scada Daten mit Filter
%plot(c,k,'r') %Interpolierte Scada Daten -> LK_scada
plot(xrange, interpol_gar, 'LineWidth',2) %Interpolierte garantierte LK ->
    LK_gar
%plot(c,l,'k') %linear grob geglättete interpolierte Scada Daten (auf 0.4er
     Schritte)
%plot(r,neu, 'x') %erneut interpoliert, dabei Auflösung erhöht auf 0.1er
    Schritte
plot(xrange,scada,'r', 'LineWidth',2) %erweitert LK_scada auf Datenbereich
    bis 25 m/s
plot(xrange, scada_n, 'k', 'LineWidth',2) %LK_scada normiert bis 25 m/s
legend('data points', 'guaranteed Pc', 'scada Pc', 'normalized scada Pc','
    Location','best')
xlabel('Wind Speed m/s')
ylabel('Power kW')

```

```
figure
hold on
plot(xrange, interpol_gar, 'LineWidth',2)
plot(xrange,scada_n, 'r', 'LineWidth',2)
plot(xrange,interpol_lidar_bin_n, 'k', 'LineWidth',2)
%plot(xrange,lidar)
legend('guaranteed Pc','normalized scada Pc', 'normalized lidar Pc (bins)','Location','best')
xlabel('Wind Speed m/s')
ylabel('Power kW')

%Weibull Verteilung
%Formparameter k
k=2
%Skalierungsfaktor A (bestimmt arithm. Geschwindigkeitsmittelwert, für 6.3 m/s entsprechend 7.11)
A=7.11
vv=0:0.1:25;
wdf=(k/A)*((vv/A).^(k-1)).*(exp(-((vv/A)).^k))
figure
plot(vv,wdf, 'LineWidth',2)
windenergy=sum(wdf.*(vv.*vv.*vv))
legend('Weibull Distribution','Location','best')
xlabel('Wind Speed m/s')
ylabel('Probability Density')

%Energieertrag
%Verfügbarkeit
eta=0.97
%garantierte Kurve
E_gar_l=interpol_gar.*wdf/sum(wdf);
P_gar_av=sum(E_gar_l)
h_volllast_g=P_gar_av/1800*365*24
E_gar=P_gar_av*365*24*eta
%Scada
E_scada_l=scada.*wdf/sum(wdf);
P_scada_av=sum(E_scada_l)
h_volllast_s=P_scada_av/1800*365*24
E_scada=P_scada_av*365*24*eta

%Scada normiert
E_scada_l_n=scada_n.*wdf/sum(wdf);
P_scada_av_n=sum(E_scada_l_n)
h_volllast_s_n=P_scada_av_n/1800*365*24
E_scada_n=P_scada_av_n*365*24*eta

%Lidar interpoliert
E_l_i_l=lidar.*wdf/sum(wdf);
P_l_i_av=sum(E_l_i_l)
h_volllast_i_l=P_l_i_av/1800*365*24
```

```
E_l_i=P_l_i_av*365*24*eta

%Lidar Method of Bins
E_l_b_l=interpol_lidar_bin.*wdf/sum(wdf);
P_l_b_av=sum(E_l_b_l)
h_volllast_b_l=P_l_b_av/1800*365*24
E_l_b=P_l_b_av*365*24*eta

%Lidar Method of Bins normiert
E_l_b_l_n=interpol_lidar_bin_n.*wdf/sum(wdf);
P_l_b_av_n=sum(E_l_b_l_n)
h_volllast_b_l_n=P_l_b_av_n/1800*365*24
E_l_b_n=P_l_b_av_n*365*24*eta

figure
hold on
plot(xrange, E_gar_l, 'LineWidth',2)
plot(xrange, E_scada_l_n, 'r', 'LineWidth',2)
%plot(xrange, E_scada_l, 'r')
plot(xrange, E_l_b_l_n, 'k', 'LineWidth',2)
%plot(xrange, E_l_b_l, 'k')
legend('based upon guaranteed Pc', 'based upon normalized scada Pc', 'based
    upon normalized lidar Pc (bins)','Location','best')
xlabel('Wind Speed m/s')
ylabel('Energy Distribution')


%Ausgabe
E=0:4
%Skalierung auf Prozent
Egar=100
Escadan=E_scada_n/E_gar*100
Elbn=E_l_b_n/E_gar*100
Escada=E_scada/E_gar*100
Elb=E_l_b/E_gar*100

E(1,1)=Egar
E(1,2)=Escadan
E(1,3)=Elbn
E(1,4)=Escada
E(1,5)=Elb

figure
bar(E)
set(gca,'XTickLabel',{'Guaranteed','Scada norm.','Lidar norm.','Scada', '
    Lidar'})
ylabel('Energy Yield')

end
```

Listing 11.1: Matlab Code

VBA Codes

Horizontal Wind Profile

```
Private Sub CommandButton1_Click()
Cells(3, 200) = 0
Cells(4, 200) = 0
Cells(5, 200) = 0
Cells(6, 200) = 0
Cells(7, 200) = 0
Cells(8, 200) = 0
Cells(9, 200) = 0
Cells(10, 200) = 0
Cells(11, 200) = 0
c = 0

For a = 3 To 13241
If (Cells(a, 197) = 0) Then
Cells(3, 200) = Cells(3, 200) + Cells(a, 26)
Cells(4, 200) = Cells(4, 200) + Cells(a, 45)
Cells(5, 200) = Cells(5, 200) + Cells(a, 64)
Cells(6, 200) = Cells(6, 200) + Cells(a, 83)
Cells(7, 200) = Cells(7, 200) + Cells(a, 102)
Cells(8, 200) = Cells(8, 200) + Cells(a, 121)
Cells(9, 200) = Cells(9, 200) + Cells(a, 140)
Cells(10, 200) = Cells(10, 200) + Cells(a, 159)
Cells(11, 200) = Cells(11, 200) + Cells(a, 178)
c = c + 1
End If
Cells(12, 200) = c

Next

Cells(13, 200) = c
Makro1

End Sub

Sub Makro1()
'
' Makro1 Makro
' Makro am 10.09.2010 von ch aufgezeichnet
'

'
    Range("GR3:GR11").Select
    Selection.Copy
    Range("GS3").Select
    ActiveSheet.Paste
    Application.CutCopyMode = False
```

```
End Sub
```

Listing 11.2: Horizontal Wind Profile Code

Method of Bins

```
Private Sub CommandButton1_Click()
v = 0
Length = Cells(8, 11)

For a = 0 To 50
b = a + 2
v = v + 0.5
Cells(b, 12) = v - 0.5
Cells(b, 14) = 0
Cells(b, 15) = 0
c = 0
For a1 = 3 To Length + 3
If (Cells(a1, 5) < v - 0.25 And Cells(a1, 5) >= (v - 0.75)) Then
c = c + 1
Cells(b, 14) = Cells(b, 14) + Cells(a1, 5)
Cells(b, 15) = Cells(b, 15) + Cells(a1, 6)
End If
Next
Cells(b, 13) = c
Next

End Sub


Private Sub CommandButton2_Click()
v = 0
Length = Cells(8, 11)

For a = 0 To 50
b = a + 2
v = v + 0.5
Cells(b, 47) = v - 0.5
Cells(b, 49) = 0
Cells(b, 50) = 0
c = 0
For a1 = 3 To Length + 3
If (Cells(a1, 32) < v - 0.25 And Cells(a1, 32) >= (v - 0.75)) Then
c = c + 1
Cells(b, 49) = Cells(b, 49) + Cells(a1, 32)
Cells(b, 50) = Cells(b, 50) + Cells(a1, 33)
End If
Next
Cells(b, 48) = c
Next
```

```
End Sub
```

Listing 11.3: Method of Bins Code